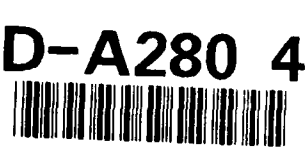

AIR FORCE OFFICE OF SCIENTIFIC RESEARCH
Contract F49620-91-C-0093

Final Technical Report
May, 1994

DEFECT INITIATION/GROWTH AND ENERGY DISSIPATION INDUCED BY DEFORMATION AND FRACTURE

J. Thomas Dickinson
Washington State University

Department of Physics and
Materials Science Program
Pullman, WA 99164-2814
(509) 335-4914
jtd@wsuvm1.csc.wsu.edu

UNCLASSIFIED

SECURITY CLASSIFICATION OF THIS PAGE

REPORT DOCUMENTATION PAGE

Form Approved OMB No. 0704-0188

1a. REPORT SECURITY CLASSIFICATION: UNCLASSIFIED

1b. RESTRICTIVE MARKINGS:

2a. SECURITY CLASSIFICATION AUTHORITY:

2b. DECLASSIFICATION / DOWNGRADING SCHEDULE:

3. DISTRIBUTION / AVAILABILITY OF REPORT: APPROVED FOR PUBLIC RELEASE DISTRIBUTION UNLIMITED

4. PERFORMING ORGANIZATION REPORT NUMBER(S): FRACTO1994

5. MONITORING ORGANIZATION REPORT NUMBER(S): AFOSR-TR- 94 0357.

6a. NAME OF PERFORMING ORGANIZATION: WASHINGTON STATE UNIVERSITY

6b. OFFICE SYMBOL (If applicable):

7a. NAME OF MONITORING ORGANIZATION: AIR FORCE OFFICE SCIENTIFIC RESEARCH DIRECTORATE OF AEROSPACE SCIENCES

6c. ADDRESS (City, State, and ZIP Code): WASHINGTON STATE UNIVERSITY PULLMAN, WA 99164-2814

7b. ADDRESS (City, State, and ZIP Code): AFOSR/NA BLDG 410 BOLLING AFB DC 20332-6448

8a. NAME OF FUNDING / SPONSORING ORGANIZATION: AFOSR/NA

8b. OFFICE SYMBOL (If applicable): NA

9. PROCUREMENT INSTRUMENT IDENTIFICATION NUMBER: F49620-91-C-0093

8c. ADDRESS (City, State, and ZIP Code): BOLLING AFB DC 20332-0001

10. SOURCE OF FUNDING NUMBERS

PROGRAM ELEMENT NO.	PROJECT NO.	TASK NO.	WORK UNIT ACCESSION NO.
61102F	2302	DS	

11. TITLE (Include Security Classification): DEFECT INITIATION/GROWTH AND ENERGY DISSIPATION INDUCED BY DEFORMATION AND FRACTURE

12. PERSONAL AUTHOR(S): J. THOMAS DICKINSON

13a. TYPE OF REPORT: FINAL TECHNICAL

13b. TIME COVERED: FROM 12/15/92 TO 12/14/93

14. DATE OF REPORT (Year, Month, Day): MAY 15, 1994

15. PAGE COUNT: 48

16. SUPPLEMENTARY NOTATION:

17. COSATI CODES		
FIELD	GROUP	SUB-GROUP

18. SUBJECT TERMS (Continue on reverse if necessary and identify by block number): DEFORMATION, CRACK PROPAGATION, FRACTURE, PARTICLE EMISSION, FRACTO-EMISSION, INTERFACIAL FAILURE, CRAZING, ELECTRICAL TRANSIENTS, MICRO-CRACKING, CONTACT CHARGING, FRACTOGRAPHY, SCANNING TUNNELING MICROSCOPY, ATOMIC FORCE MICROSCOPY, PHOTOLUMINESCENCE, CHEMISORPTIVE ELECTRON EMISSION.

19. ABSTRACT (Continue on reverse if necessary and identify by block number)

Based on our capabilities to a) detect and characterize particle release from surfaces on fast time scales, b) to measure rapid electrical transients, and c) to obtain high resolution topographical information utilizing scanning tunneling and atomic force microscopy, we have investigated a number of defect initiation and growth processes which ultimately leads to fracture and energy dissipation. We employ dynamic methods as well as post-fracture examination in polymers, ceramics, metals, and interfaces. We have examined mechanisms, with interpretation and connections between these results and the creation and evolution of defects in materials under mechanical stress. The information we are acquire with our techniques has important implications concerning dissipation of energy (e.g., plastic deformation, microcracking, crack branching, and crack deflection) which play critical roles in controlling the strength and toughness of materials.

20. DISTRIBUTION / AVAILABILITY OF ABSTRACT: ☒ UNCLASSIFIED/UNLIMITED ☐ SAME AS RPT. ☐ DTIC USERS

21. ABSTRACT SECURITY CLASSIFICATION: UNCLASSIFIED

22a. NAME OF RESPONSIBLE INDIVIDUAL: W. F. Jones

22b. TELEPHONE (Include Area Code): 202 767-0470

22c. OFFICE SYMBOL: NA

DD Form 1473, JUN 86 — Previous editions are obsolete. — SECURITY CLASSIFICATION OF THIS PAGE

UNCLASSIFIED

19 MAY 1994

I. TECHNICAL SUMMARY

During the deformation of materials, a sequence of events occurs which results from stress being applied to the inherent microstructure and flaw distributions in all materials. Eventually, these events culminate in catastrophic damage or failure. We have been probing this time sequence of events using dynamic methods as well as post-fracture examination in polymers, ceramics, metals, and interfaces. These probes include time-resolved measurements of particle emission (fracto-emission), electrical transients during interfacial failure, and the use of scanning tunneling microscopy of fracture surfaces These studies include recently developed techniques utilizing chemisorptive electron emission (CSE) to quantify the degree of plastic deformation of metals during fracture at metal/ceramic interfaces. This report summarizes our results in these areas and provides a list of generated publications and manuscripts. These results have important implications concerning dissipation of energy (e.g., plastic deformation, microcracking, crack branching, and crack deflection) which play critical roles in controlling the strength and toughness of materials.

II. SUMMARY OF WORK UNDER CONTRACT F49620-91-C-0093.

The major areas where we have focused our studies include the use of chemisorptive electron emission to probe plastic deformation in metals including fracture of metal-ceramic interfaces, the use of electron and photon emission as a measure of fracture phenomena in polymers, neutral emissions as a probe of fracture and deformation in polymers and ceramics, electrical transient measurements to examine interfacial crack growth, scanning microscopies applied to the study of fracture surfaces, and the use of photoluminescence to examine the build up of defects in crystalline materials. Our goals have been to develop new time-resolved tools for determining the onset and extent of damage and energy dissipation during deformation and fracture. We present short summaries of these studies. We also present a list of publications and invited talks associated with the research sponsored under this contract.

Chemisorptive Electron Emission as a Probe of Deformation

Chemisorptive electron emission as a probe of plastic deformation in reactive metals. The surface area created during tensile deformation and fracture of the reactive metals Ti, Zr, Mg, and Al was probed by real-time measurements of chemisorptive electron emission (CSE) due to oxygen adsorption. CSE was shown to be sensitive to the number of fresh metal atoms exposed at the surface as a consequence of plastic deformation. At constant strain rate, Ti, Zr, and Mg all displayed exponential increases in CSE intensities during loading, reflecting exponential increases in surface area prior to fracture. In Ti and Zr, CSE began at the onset of unstable necking. In contrast, CSE intensities from Al reflect a nearly constant rate of surface area production during deformation at constant strain rate. Calibration of the Ti CSE intensities per unit surface area allowed determination of the total surface area produced during deformation and fracture. Atomic force microscopy of the necked region in strained Ti samples showed dramatic increases in surface roughness, in near agreement with the CSE results. A model was developed to account for these

observations. The utility of CSE measurements as a probe of deformation and ductile fracture has been demonstrated.

Chemisorptive electron emission as a probe of deformation during fracture of a metal/glass interface. We performed measurements of the electron emission intensity accompanying the reaction of metallic magnesium with oxygen following the peel of 1-μm thick magnesium films from soda lime glass. The resulting emission intensities are strongly correlated with the total peel energy, consistent with a close relation between the emission intensities and the deformation processes. Atomic force microscopy (AFM) of the peeled magnesium surfaces indicate that surfaces yielding weak emissions and low peel energies are very smooth. In contrast, angular voids are observed on surfaces which yield weak emissions and high peel energies. The weak emissions accompanying the peel of samples yielding the lowest peel energies indicate that very little metallic Mg is exposed, consistent with fracture through an interphase material. Deformation processes, when they occur, raise the peel energy and expose metallic Mg to the ambient oxygen, resulting in electron emission. The relation between surface roughness as observed by AFM and the deformation processes have been analyzed and are also consistent with energy dissipation during interfacial crack growth being dominated by metal plasticity, although the correlations are not as satisfying as with CSE. **Because this work is our current area of focus and we are enthusiastic about continuing it, we have included in Appendix I a preprint of a manuscript detailing these Mg/glass results.**

Photon and Electron Emission from Polymers

FE from HDPE: Bond Breaking vs Tribological Stimulation. We have re-examined the emission of electrons and positive ions from high density polyethylene (HDPE) during tensile deformation at strain rates on the order of 30% s^{-1}. Earlier reports have suggested that electron emission due to bond scissions accompanying deformation of

HDPE have been observed. We examined the role of small frictional effects on the polymer at the edges of the clamps due to slippage during elongation. We have shown that when slippage is eliminated, the deformation-induced particle emission vanishes. Thus the pre-failure electron and positive ion emission is not due to bond scissions as a result of tensile deformation of the polymer but to slippage of the polymer in the grips. We have examined the processes occurring during tribological loading which produce intense, longer lasting emission during and after stimulation. We show that the emission due to tribological loading involves charge transfer upon contact between metal and polymer, mechanical separation of charge, and subsequent dynamic stimulation of the polymer surface due to energetic charge motion (surface flashover).

EE and phE accompanying deformation and fracture of polycarbonate. Electron and photon emission accompanying tensile loading and failure of polycarbonate showed relatively weak emissions during the onset of neck formation and intense emissions during the fracture event itself. These results are interpreted in terms of formation of active species by bond breaking followed by emission driven by energy released by recombination. Fast time scale measurements *during* fracture indicate that intense electron and photon emission typically begins about 50 μs prior to the completion of fracture and is most intense at the completion of fracture. The gradual onset reflects the final stages of growth of the failure-initiating defect. Defect growth was monitored by measuring the intensity of a light beam transmitted through the gauge length of the sample; the transmission is sensitive to scattering by surface and bulk defects. A marked decrease in transmission begins some tens of ms prior to fracture due to scattering from the fracture-initiating defect. These measurements allow accurate correlations of defect growth with the onset of the electron and photon signals.

PhE during deformation and glass-fiber-reinforced bisphenol-A-polycarbonate. We give a survey on mechanically induced emission phenomena (acoustic emission [AE], neutral particle emission [NE], electron and charged particle emission [EE/PIE], radio wave

emission [RE] of polymers and briefly summarize these effects in unfilled and glass-fiber-reinforced bisphenol-A-polycarbonate. A general treatment of the photon emission kinetics in terms of analysis and description, using a convolution function, is proposed. The kinetics obey a power law decay in time. By examining a model mechanism for the interfacial failure of the composite, i.e., by peeling of glass-polymer laminates, we show that the origin of the photon emission is the polycarbonate matrix after cleavage of the glass/polymer interface. Spectral characteristics of mechanically induced luminescence of glass-filled polycarbonate and of the peeling spectra of the model system of glass/polycarbonate laminates are discussed. Different brands of polycarbonate yield identical spectra. Spectra recorded during peel in vacuum are very similar to those recorded during deformation of the composite. Polarized fluorescence spectroscopy and electron-beam luminescence were used to obtain further information about the intrinsic polycarbonate-chromophores that are available for mechanically induced photon emissions.

Recombination on fractal networks: PhE and EE following fracture of materials. We report measurements and analysis of fracture-induced photon and electron emissions from several polymeric and inorganic systems on times scales of 10^{-2} to 10^{3} seconds following fracture. The dominate mechanism for post-fracture emission involves the recombination of mobile free carriers (usually electrons) with immobile recombination centers. The emission decays were modeled as (pseudo)unimolecular and bimolecular recombination on fractal lattices as described by Zumofen, Blumen, and Klafter. Although the decay kinetics show a great deal of variability from material to material, this random walk description of the recombination process provides an excellent description of the emissions over long time scales. This analysis shows a strong correlation between the local structure at the fracture surface and the resulting decays.

Neutral Emissions as a Probe of Fracture and Deformation in Polymers and Ceramics

Molecular CO emission accompanying fracture of polycarbonate: evidence for chain cleavage. When polycarbonate is loaded in tension at room temperature to failure, a certain percentage of the chains undergo cleavage due to the constraints of entanglements. We present direct evidence that accompanying fracture of polycarbonate, CO molecules are released due to bond scissions. We estimate the efficiency of this process.

Ar atom emission as a probe of craze formation and craze growth in polystyrene. We report measurements of Ar emission during the loading of polystyrene and high impact polystyrene in vacuum. Argon was introduced into the material prior to the experiment by storing the samples in an Ar atmosphere. The development of crazes during loading was monitored by videotaped visual observations and scattered light measurements. Increased Ar emission is observed at the onset of crazing, provided that the crazes intersect the surface. The strength of the Ar signal depends upon the extent of crazing; especially intense signals are observed from samples which display significant crazing prior to fracture. High impact polystyrene shows intense emissions at yield which soon decay due to the depletion of Ar from the near surface material. The emission intensity rises again prior to fracture, when surface crazes become connected to crazes in the bulk. Thus the emission of volatile species during deformation reflects the growth of crazes intersecting the surface, as well as changes in the "connectivity" of the craze network.

Temperature measurements of NE during the fracture of polystyrene: A determination of the fracture energy and fracture surface temperature. The emission of volatile species accompanying the fracture of polystyrene was monitored as a function of time by two quadrupole mass spectrometers mounted at different distances from the sample. The resulting time-of-arrival signals were numerically modeled to yield an estimate of the energy per unit area dissipated as heat by fracture. Neutral emissions of ethyl benzene molecules (a common volatile impurity) and a noble gas (Ar--introduced by exposure) were

monitored. Dissipation (fracture) energies were determined and ranged from 680 to 1480 J/cm^2 consistent with the range of energy release rates in the literature. The peak surface temperatures calculated from the measured heat dissipation ranged from 600 to 1300 K.

Emission of occluded volatiles during deformation of polycarbonate due to strain enhanced diffusion. Measurements of the emission of purposely entrained volatiles (Ar and D_2O) during the loading and unloading of a bisphenol-A polycarbonate in vacuum are made by quadrupole mass spectrometry. Transient loading events are accompanied by dramatic increases in emission, reflecting a similar rise in the diffusion constant of the measured species. We attribute this change to an increase in size of molecular voids in the polymer network, which accompany the increase in sample volume under load. The results are interpreted in terms of the Dolittle relation in which the diffusion constant depends exponentially upon v^*/v_{fo}, the ratio between an activation volume for diffusion and the average size of the relevant voids in the polymer network. Our data suggests that v^*/v_{fo} is unusually low in the D_2O-polycarbonate system, which we attribute to a relatively large value of v_{fo}; this would be consistent with the relatively long distance between flexible links in the polycarbonate structure.

Xenon emission accompanying fracture of xenon-implanted cubic zirconia. The emission of xenon following the fracture of xenon-implanted cubic zirconia was studied by time resolved mass spectrometry. All samples showed intense Xe bursts at failure. Order of magnitude estimates of the amount of Xe released suggest that μm-scale regions of the tensile surface on either side of the fracture surface must be substantially depleted in Xe. SEM micrographs of the tensile surface of these samples do not show sufficient damage to account for this emission. However, SEM micrographs of the fracture surface show evidence for extensive microcracking immediately adjacent to the tensile surface. It is believed that these microcracks are formed when the advancing crack encounters the tensile stresses immediately below the Xe-implanted surface layer and disrupts the Xe inclusions produced by implantation. Some samples also show Xe bursts prior to failure; SEM

observations of these samples show shallow conchoidal cracks on the tensile surface which apparently form during loading and would account for the release of Xe prior to failure.

Electrical Transients as a Probe of Interfacial Crack Growth

Electrical transients generated by the peel of a pressure sensitive adhesive from a copper substrate. Part I: Initial Observations. The formation of adhesive bonds is generally accompanied by contact electrification. When these bonds are subsequently broken, the resulting charge separation can produce transient electrical signals and even electrical discharges. We present detailed measurements of electrical currents generated by peeling a pressure sensitive adhesive (PSA) from an electropolished Cu substrate in air and in vacuum. The magnitude of these currents depends strongly upon rate of interfacial failure along the peel front. Transient fluctuations in the rate of interfacial failure at the peel front are shown to result in fluctuations in the measured current. Intense current spikes due to electrical breakdown events are also observed. We have characterized these breakdown events in various atmospheres by the current signals and long-wavelength electromagnetic radiation, as well as spectroscopy of the accompanying light emission. Current measurements are a potentially new time-resolved probe of micromechanical and electrical processes accompanying peeling.

Electrical transients generated by peeling a pressure sensitive adhesive from a copper substrate. Part II: Analysis of fluctuations—evidence for chaos. We report measurements of the electrical current fluctuations generated by peeling a pressure sensitive adhesive from a smooth, clean copper substrate in the ~180° peel geometry at speeds between 2 and 6 mm/s. Spectral analysis of these fluctuations using Fourier transform techniques reveal broad bands in the region of 0-150 Hz at these peel speeds. A significant transition in the spectral behavior is observed at peel speeds between 4 and 6 mm/s. The general appearance, spectral behavior, and autocorrelation functions of the fluctuations are

all suggestive of chaos. Dimensional analysis of the current signals indicate that the fluctuations are associated with a strange (fractal) attractor of dimension 5.5-5.6. The finite dimension rules out the possibility that these fluctuations are random. The close relation between the current signals and the mechanical events accompanying peeling suggest that peel event itself is fractal in a spatial-temporal sense, and therefore chaotic in nature.

Scanning Microscopies Applied to Fracture Surfaces.

STM Observations of Polymer Fracture Surfaces. Scanning tunneling observations of gold-coated polymer fracture surfaces are reported. We compare nm-scale surface features of poly(methyl methacrylate) (PMMA) fractured under three different loading conditions: in tension at room temperature, in tension at liquid nitrogen temperature, and in the double torsion geometry at room temperature (slow crack growth). Fracture surfaces of polystyrene and polycarbonate loaded in tension at room temperature are also described. Each of these surfaces shows distinctive nm-scale features which we interpret in terms of the interactions between craze growth (fibril formation) and crack growth along the craze boundary. The resolution of these images is sufficient to greatly complement other fractographic studies.

STM Observations of Metallic Glass Fracture Surfaces. We have performed scanning tunneling microscope observations of fracture surfaces formed during catastrophic crack growth in three metallic glasses: $Ni_{56}Cr_{18}Si_{22}B_4$, $Co_{69}Fe_4Ni_1Mo_2B_{12}Si_{12}$, and $Fe_{78}B_{13}Si_9$. Macroscopically, the first two glasses fail along a slip band formed during loading and display a characteristic, μm-scale pattern of vein-like ridges; in contrast, $Fe_{78}B_{13}Si_9$ displays little slip prior to fracture and its fracture surface shows a μm-scale chevron pattern of steps. STM observations of fracture surfaces of all three materials show nm-scale grooves. The grooves in $Co_{69}Fe_4Ni_1Mo_2B_{12}Si_{12}$ are especially prominent and display stepped edges which we attribute to the intersection of shear bands with the surface.

STM observations of the vein-like features on $Ni_{56}Cr_{18}Si_{22}B_4$ also show stepped edges. We attribute the vein features to the interaction of adjacent crack fingers in which the material between adjacent fingers fails in plane stress. The origin of the grooves is uncertain, but may be due to other shear instabilities along the crack front.

STM Observations of the Mirror Region of Silicate Glass Fracture Surfaces. We report scanning tunneling microscope images of gold-coated fracture surfaces of soda lime glass and fused silica in the mirror region. The scans show a variety of nanometer scale features that are attributed to fracture phenomena at this scale. We find considerable similarity to the structures observed in regions of macroscopic extensive crack branching (e.g., "mist"). The density of the "nanomist" features increases as one progresses away from the crack origin towards the mirror-mist boundary. Comparisons are made between soda lime glass and fused silica, revealing differences in the local deformation behavior of these two materials. Self-similarity of the observed structures is probed by measurements of the fractal dimension, D_f, of the surfaces created in soda lime glass near the mirror-mist boundary, where we observe $2.17 < D_f < 2.40$.

Changes in air-exposed fracture surfaces of silicate glasses observed by AFM. We have produced atomic force microscope images of fracture surfaces of soda-lime glass, barium-borosilicate glass, and fused silica, fractured in low vacuum and subsequently exposed to humid air. Our observations reveal that (1) soda-lime glass fracture surfaces exposed to air develop swellings 50-70 nm high after three days, while vacuum stored samples show protrusions less than 10 nm high; with continued exposure to humid air, these swellings disappear and cone-like structures are formed; (2) barium-borosilicate fracture surfaces exposed to air develop relatively small numbers of crystalline protrusions typically 65 nm high after three days, while no similar features are observed on vacuum-stored material; and (3) fused silica fracture surfaces exposed to humid air for three days show no significant surface features when compared to vacuum-stored material. The nm-scale structures observed on air-exposed fracture surfaces of soda-lime silica and barium-

borosilicate are attributed to interactions between alkali and/or alkaline-earth cations in the material and water + CO_2 from the air.

Other Effects

Photoluminescence imaging of mechanically produced defects in MgO. Deformed MgO displays a strong blue photoluminescence when illuminated by 248 nm excimer laser radiation. This photoluminescence is readily imaged in situ (during laser exposure) using commercial microscope optics. We report photoluminescence images of indented, cleaved, abraded, and laser-damaged surfaces and relate the observed features to the expected deformation patterns. Locally deformed regions on MgO single crystals are sites of localized absorption at 248 nm and serve to nucleate localized damage under high fluence irradiation. Photoluminescence imaging has great potential for the identification of flaws in optical materials prior to, during, and after exposure to damaging fluences of laser radiation and for fundamental studies of deformation, fracture, and tribology.

Structures obtained from resolidification of flame melted single crystal germanium. When single crystal germanium is partially melted with a gas flame in air, resolidification produces novel structures which may be useful for nanoscale fabrication. These features are dominated by a single, sharp cone 1-5 mm long, with a typical aspect ratio of 1.6. If impurity concentrations are sufficiently high, one or more micron-sized, impurity-rich spheres are formed at the tip of the cone. The surface displays a distinctive morphology which depends strongly on the chemical environment. Under conditions of slower resolidification in air, the cone body and spheres are coated with fractal-like aggregates of spherical oxide particles. The observed features are attributed to dynamic resolidification, impurity segregation, and diffusion limited aggregation processes.

III. List of Papers Sponsored by AFOSR

"Scanning Tunneling Microscope Observations of Polymer Fracture Surfaces," D. M. Kulawansa, S. C. Langford, and J. T. Dickinson, J. Mater. Res. 7, 1292 (1992).

"Observations of Fracture Surfaces in Metallic Glasses by SEM and STM," Y. Watanabe, J. T. Dickinson, D. M. Kulawansa, and S. C. Langford, Memoirs of the Japanese Defense Academy, 31(2) pp. 53-59, (1992).

"Time-resolved electrical transient measurements during failure between polymer-metal interfaces," J. T. Dickinson, Polym. Prepr. (Am. Chem. Soc, Div. Polym. Chem.) 34(2), 272 (1993).

"Recombination on fractal networks: photon and electron emission following fracture of materials," J. T. Dickinson, L. C. Jensen, and S. C. Langford, J. Mater. Res. 8(11), 2921 (1993).

"Ar atom emission as a probe of craze formation and craze growth in polystyrene," J. T. Dickinson, L. C. Jensen, S. C. Langford, and R. P. Dion, J. Polym. Sci.: Polym. Physics Ed. 31, 1441 (1993).

"Excitations produced during fracture of polymers and interfaces," J. T. Dickinson, Polym. Prepr. (Am. Chem. Soc, Div. Polym. Chem.) 34(2), 254 (1993).

"Scanning Tunneling Microscope Observations of Metallic Glass Fracture Surfaces," D. M. Kulawansa, J. T. Dickinson, and S. C. Langford, and Y. Watanabe, J. Mater. Research 8, 2543 (1993).

"Electron and photon emission accompanying deformation and fracture of polycarbonate," K. A. Zimmerman, S. C. Langford, J. T. Dickinson, and R. P. Dion, J. Polym. Sci.: Part B: Polym. Physics Ed. 31, 1229 (1993).

"Photon Emission during deformation of glass-fiber reinforced bisphenol-A-Polycarbonate," J. Fuhrmann, L. Nick, J. T. Dickinson, and L. C. Jensen, J. Appied Polym. Sci. 48, 2123 (1993).

"Xenon emission accompanying fracture of xenon-implanted cubic zirconia," M. G. Norton, Wenbiao Jiang, J. T.Dickinson, L. C. Jensen, S. C. Langford, E. L. Fleischer, and J. W. Mayer, J. Am. Ceram. Soc. 76, 2076 (1993).

"Fracto-Emission from High Density Polyethylene: Bond Breaking vs Tribological Stimulation," J. T. Dickinson, L. C. Jensen, and R. P. Dion, J. Appl. Phys. 73, 3047 (1993).

"Chemisorptive electron emission as a probe of plastic deformation in reactive metals," J. T. Dickinson, L. C. Jensen, S. C. Langford, and R. G. Hoagland, J. Mater. Res. 9, 1156 (1994).

"Scanning tunneling microscope observations of the mirror region of silicate glass fracture surfaces," D. M. Kulawansa, L. C. Jensen, S. C. Langford, and J. T. Dickinson, and Y. Watanabe, J. Mater. Res. 9, 476 (1994).

"Emission of occluded volatiles during elastic deformation of polycarbonate," J. T. Dickinson, L. C. Jensen, S. C. Langford, and R. P. Dion, J. Polym. Sci.: Polym. Physics Ed. 32, 993 (1994).

"Temperature measurements of the gaseous emission during the fracture of polystyrene: a determination of the fracture energy and fracture surface temperature," J. T. Dickinson, L. C. Jensen, S. C. Langford, and R. P. Dion, J. Polym. Sci.: Polym. Physics Ed. 32, 779 (1994).

"Changes in air-exposed fracture surfaces of silicate glasses observed by atomic force microscopy," Yoshihisa Watanabe, Yoshikazu Nakamura, J. T. Dickinson, and S. C. Langford, to appear in J. Non-Cryst. Solids.

"Electrical transients generated by the peel of a pressure sensitive adhesive from a copper substrate. Part I: Initial Observations," Sunkyo Lee, L. C. Jensen, S. C. Langford, and J. T. Dickinson, submitted to J. Adhes. Sci. Technol.

"Electrical transients generated by the peel of a pressure sensitive adhesive from a copper substrate. Part. II. Analysis of fluctuations," Louis Scudiero, J. T. Dickinson, L. C. Jensen, and S. C. Langford, submitted to J. Adhes. Sci. Technol.

"Structures obtained from resolidification of flame melted single crystal germanium," M. L. Dawes, J. T. Dickinson, L. C. Jensen, and S. C. Langford, submitted to Nanotechnology.

"Chemisorptive electron emission accompanying peel of thin Mg films from soda lime glass," Sumio Nakahara, J. T. Dickinson, and S. C. Langford, manuscript in preparation, to be submitted to J. Mat. Research.

IV. Invited Talks Related to AFOSR Work

Molecular Emissions From Bond-Scissions in Polymers," Dow Chemical Co., August, 1991.

Eight Lectures on "Dynamic Processes at Surfaces" Japan Defense Agency, Sept-Oct. 1991.

"Fracto-Emission: Recent Studies in Particle Emission Accompanying Interfacial Failure," Osaka University, Osaka, Japan, October, 1991.

"The Origin and Evolution of Defects in Materials Under Stress," AFOSR Workshop on Defects, Wright-Patterson, October, 1991.

"Fundamental Processes Accompanying Fracture of Polymers and Interfaces," 3M Corporation, October, 1991.

"Fracto-Emission: Recent Studies in Particle Emission Accompanying Interfacial Failure," Dept. of Physics, Western Michigan University, Kalamazoo, Nov. 1991.

"Fracto-Emission from Ceramics and Glasses," American Ceramics Society, Minneapolis, April, 1992.

"Chaos and Fractals in Fracture", Gordon Conference on Fractals, June, 1992.

"Mechanisms for Ablation of Insulators," DOE Workshop-Lasers in Chemistry, Sante Fe, October, 1992.

"Mechanical Consequences of Laser Bombardment of Insulators", Workshop on Dynamic Response of Materials to Energy Deposition, Los Alamos, January, 1993.

"The Detection of Crazing and Microcracking in Strained Polymers", Dow Co., February, 1993.

"Fracto-Emission from Polymer Interfaces," ACS Symposium on Adhesion, Chicago, August, 1993.

"Deformation and Fracture Induced Luminescence Phenomena in Polymers," ACS Symposium on Polymers, Chicago, August, 1993.

"Transient Electrical Measurements of Adhesive Failure," 3M Co., October, 1993.

"Fracto-Emission Studies in Polymers," Department of Materials Science, University of Michigan, October, 1993.

"Dissipative Processes in the Fracture of Crystalline Materials," International Symposium on Fracture and Strength of Glass and Ceramic Materials, PAC-RIM 1993, Honolulu, Nov., 1993.

"Luminescence and Mass Spectroscopic Probes of Deformation and Fracture," American Ceramics Society, Indianapolis, April, 1994.

To be presented:

"New Studies in Fracto-Emission," Lectures at TU and FU, Berlin, Germany, Spring, 1994.

"Energetic Processes at Glass Surfaces," Gordon Conference on Glass, June, 1994.

"Mechanisms of Laser Ablation of Wide Band Gap Materials," Gordon Conference on Laser Ablation, August, 1994.

"Fractals and Chaos in Fracture," MRS, Boston, November, 1994.

"Deformation and Fracture Probes in Polymers and Interfaces," MRS, Boston, November, 1994.

"Atomic/Molecular Processes associated with fracture", 4 Lectures, Mechanical Engineering Laboratory, Tsukuba-City, Japan, January, 1995.

Appendix I

Chemisorptive electron emission and atomic force microscopy as probes of plastic deformation during fracture at a metal/glass interface

Sumio Nakahara,* S. C. Langford, and J. T. Dickinson

Physics Department, Washington State University, Pullman, WA 99164-2814 USA

We examine the use of chemisorptive electron emission (electron emission accompanying the adsorption of a reactive gas on a metal surface) and atomic force microscopy as measures of plastic deformation during fracture at a metallic Mg/glass interface. Localized ductile deformation in the metallic phase, which enhances the fracture energy, exposes metallic Mg to the reactive O_2 atmosphere, producing intense emissions. The number of electrons emitted following fracture in low-pressure oxygen atmospheres is strongly correlated with the total energy expended during failure (peel energy). The presence of localized ductile deformation in the high peel energy samples is verified by atomic force microscopy (AFM): angular voids are observed on surfaces yielding high fracture energies and intense emissions; these voids are not observed on samples yielding the lowest peel energies and emission intensities. Quantitative use of roughness derived from the AFM data is, however, problematic. The potential for the use of chemisorptive electron emission as a probe of deformation at interfaces involving Mg, Ti, Zr, and Al is promising.

*Permanent Address: Department of Mechanical Engineering, Kansai University, 3-3-35 Yamatecho, Suita, Osaka 564, Japan

Keywords: metal-ceramic interfaces, metal plasticity, adhesion, fracture energy, chemisorptive electron emission, atomic force microscopy

INTRODUCTION

Plastic deformation in the metallic phase of ceramic-metal composites often makes a dominant contribution to the energy required for fracture. In particular, the amount of deformation exhibited by the metallic phase is a strong function of the tortuosity or roughness of the interface,[1,2] the thickness of the metallic phase,[3,4] and the presence of interphase materials.[3] At present, the chief means of estimating the contribution of deformation to the measured toughness of ceramic-metal composites involves careful fractographic examination and numerical modeling. More direct methods are of course desirable, and are especially important where ductile deformation of the metallic phase and brittle fracture at or near the interface occur simultaneously.[5,6] In this work, we exploit the phenomenon of chemisorptive emission (CSE—electron emission accompanying the adsorption of reactive gases with clean metal surfaces) to provide such a probe.

In a previous study,[7] we showed the CSE was a sensitive measure of plasticity in tensile deformation of a number of metals. In principle, the method has some similarity to previous attempts to use photoelectron emission to examine tensile deformation[8] and fatigue damage[9] in metals such as Al and Mg. Steps produced by the intersection of dislocations with the surface increase the surface area of the low work function metallic phase and thus increase the photoelectron emission intensities. The chief advantage of CSE in this regard is its uniform sensitivity to deformation in a variety of sample geometries. Gas molecules tend to be adsorbed uniformly on complex surfaces, whereas in photoelectron measurements, portions of the surface are often shadowed from the uv light. The presence of thin oxide layers on undeformed material prevents CSE (which requires adsorption on fresh metal), whereas uv photons and photoelectrons can penetrate sub-μm oxides to produce intense signals even in the absence of deformation. Thus, CSE is a superior probe of surface roughness generated by plastic deformation.

EXPERIMENT

The experiments were performed in two stainless steel vacuum systems with base pressures less than 1×10^{-5} and 1×10^{-7} Pa, respectively. A schematic of the experimental arrangement is shown in Fig. 1(a). Total pressures were measured with Bayard-Alpert ionization gauges. Oxygen was used as the reactive gas and was leaked into the system through a clean manifold and leak valve, raising the pressure in the vacuum system to 4×10^{-4} Pa. Electron emission was detected with a Channeltron electron multiplier (CEM), Galileo Electro-optics Model 4039. The front cone of the CEM was biased at +1000 V to attract and efficiently detect electrons. Within about 2 s after the completion of peel, the two sides of the sample were drawn away from each other, allowing for efficient detection of electrons emitted from the Mg surface.

The CSE intensity as a function of Mg surface area was calibrated by exposing a freshly evaporated film of magnesium to oxygen. A Mg thin film was evaporated onto a glass substrate at a background pressure of 3×10^{-6} Pa. The substrate was then rotated to face a CEM while the O_2 pressure was rapidly raised to 4×10^{-4} Pa. The resulting total yield from magnesium films was 3×10^{8} electrons/cm^2 which corresponds to a yield of 1×10^{-7} electrons/Mg surface site. Atomic Force Microscope (AFM) observations of the evaporated film with a Digital Instruments Nanoscope III confirm that the roughness of the film was negligible; (the ratio between the total surface area and the projected surface area was 1.03).

Magnesium/glass interfaces were formed by evaporating thin Mg films onto clean glass slides in vacuum. The glass slides were first cleaned by washing for fifteen minutes in acetone with ultrasonic agitation, followed by a similar treatment in methanol; the slides were then rinsed by condensing steam onto the surface and allowing the condensate to drip off. The slides were then mounted in an ion-pumped deposition system with a base pressure of $< 1 \times 10^{-5}$ Pa. Deposition was performed by evaporation from a resistively heated molybdenum boat mounted about 15 cm from the glass slide which was maintained at room temperature. Thermocouples mounted to the glass slide on several runs indicated that the substrate temperature rose no more

than 20 °C during deposition. During deposition, the pressure typically rose to about 8×10^{-4} Pa. The film thickness was monitored by a quartz microbalance positioned near the glass slide.

Small angle x-ray scattering measurements on a 1–μm film indicated a high degree of orientation in the polycrystalline film, with the c-axis of the grains aligned normal to the surface. A similar preferential orientation has been observed in Mg films deposited by "cluster-beam" techniques onto room temperature glass substrates.[10]

The sample geometry employed is shown in Fig. 1(b). A triangular piece of Mg-coated glass was epoxied between two other glass slides to which the load was applied. Failure initiated at the tip of the triangle and proceeded along the Mg/glass interface, the Mg remaining on the epoxy. This geometry provided a well defined defect for crack initiation, similar to that provided in chevron-notched samples. After initial "pop-in" of a small starter crack, steady crack growth followed at roughly constant load. Post-fracture analysis indicated that the starter crack represented only a small fraction (< 1%) of the total surface area. Sandwiching a ductile metal between brittle substrates, as in Fig. 1(b), minimizes the effect of residual stresses on crack growth along the great majority of the fracture surface; the film is constrained on both sides by stiff materials and therefore it is not free to deform in response to residual stresses when the crack length becomes much longer than the film thickness.[6]

The total energy expended during crack growth (here designated the peel energy) was estimated from the total area of the constant load portion of the load vs displacement curve. We note that the energy so derived is not simply related to the critical strain energy release rate at the onset of crack growth (except possibly in highly brittle materials), but represents the average energy required for surface formation during *continuous* crack growth. As the great majority of the surface is formed during continuous crack growth, the peel energy is a more appropriate measure of deformation for comparison with emission measurements.

Small portions of the Mg surface exposed by fracture were examined by AFM in the contact mode using commercial Si_3N_4 tips with nominal radii of curvature of 40 nm. The observed portions were generally taken from the base of the sample, near the completion of peel.

Similar portions of the glass substrate (from which the Mg was peeled) were also observed. Repeated observation of the Mg and glass surfaces over the course of several days showed small changes in the Mg surfaces and larger changes in the glass surfaces—most likely due to interactions with the ambient air.[11] Most of the observations described here were performed within six hours after removal from the vacuum system to minimize these effects. The images presented below have not been smoothed or otherwise processed. The mean surface roughness, R_a, of a series of AFM images was computed using the relation

$$R_a = \frac{1}{L_x L_y} \sum_{x_i=1}^{256} \sum_{y_i=1}^{256} |f(x_i,y_i)| \, \Delta x \, \Delta y \quad , \qquad (1)$$

where L_x and L_y are the dimensions of the scanned region and Δx and Δy are the distance between measurements in the x- and y-directions, respectively. $f(x_i,y_i)$ is the difference between the height measured at position (x_i,y_i) and the center plane of the scan; the center plane is determined by performing a least squares fit of a plane to the scan and displacing the plane vertically until half of the volume enclosed between it and the scan lies above the plane and half below.

RESULTS

Figure 2 shows the CSE emission intensities (log) vs time from a very high peel energy surface (a 1-μm film with a peel energy of about 16 J/m^2) and a low peel energy surface (a 0.5-μm film with a peel energy of 3.2 J/m^2). Both samples yielded intense emissions during the peel event itself, saturating the electron counting electronics. The emissions from the 0.5-μm film drop markedly after peel and continue to drop for the duration of data acquisition. Although the emissions from the 1-μm film drop two orders of magnitude in intensity after peel, they subsequently rise to high levels before beginning a long, slow decay. Furthermore, as shown in

Fig. 2(a), the emissions show a strong dependence of the partial pressure of O_2, falling sharply when the O_2 pressure is reduced, rising again when the O_2 pressure is restored. A strong pressure dependence is characteristic of CSE. In contrast, the emissions from the 0.5 μm-film are not significantly affected by changing the partial pressure of O_2, implying very small CSE intensities. Thus peeling the 0.5-μm film has exposed very little metallic Mg, consistent with failure through a brittle oxide-like interphase with few clean Mg sites exposed. In contrast, the emissions from the 1-μm film correspond to a metallic Mg surface coverage of about 16% of the nominal surface area.

The peel energy of 1-μm films ranged from about 8 to about 16 J/cm^2, and over this range the CSE emissions were strongly correlated with total peel energy as determined from the load curves. The prompt emissions have been investigated previously,[12,13] occur with or without the O_2 background, and at best weakly correlated with the peel energy (e.g., both samples in Fig. 2 show very intense emissions during peel). To reduce the influence of this emission and quantify the CSE, electron counts were integrated from 50 s to 1200 s after the onset of peeling. The resulting CSE intensities are plotted in Fig. 3 as a function of peel energy. The linear relation implies that the process responsible for the variation in peel energies also exposes metallic Mg to the surrounding atmosphere. The low peel energy point corresponding to the 0.5-μm film of Fig. 2(b) is also included in Fig. 3, along with a least squares fit to the data corresponding to the 1-μm films (i.e., omitting the 0.5-μm film point). The least squares fit to the 1-μm film data crosses the x-axis near the point corresponding to the 0.5-μm film, which yielded extremely weak emissions. Assuming that the enhanced peel energies in the 1-μm films are due to deformation in the metallic phase, the peel energy of the 0.5-μm film (about 3 J/m^2) appears to represent the "zero deformation" limit of failure in this system.

AFM images of the Mg surfaces after failure confirm the presence of ductile voiding in the high energy peel samples. Typical AFM images of high and low energy peel surfaces are shown in Fig. 4; these particular samples yielded the emissions of Figs. 2(a) and 2(b). All of the high peel energy, high emission surfaces showed large numbers of sub-μm sized voids along the

surface. The low energy peel surface is relatively smoother with no voids being observed. The voids in the high peel energy samples are typically about 10 nm deep, with relatively flat bottoms and angular sides. This geometry is consistent with slip on the (0002) basal planes of HCP Mg,[14] with the grains oriented parallel to the fracture surface (as indicated by small angle x-ray diffraction measurements). The surfaces of the high peel energy samples are not entirely uniform: one occasionally finds $2 \times 2\ \mu m^2$ regions with no holes, for instance. Nevertheless, the difference between any of the high energy peel surfaces and the low energy peel surfaces is dramatic.

Typical AFM images of the glass surfaces corresponding to the high and low peel energy Mg surfaces in Fig. 4 are shown in Fig. 5. Although the peeled glass surfaces often displays some roughness, the surface features have no relation to the voids observed on the Mg surfaces of the high energy peel samples. This implies void formation by nucleation and growth in the metallic phase, similar to the formation of ductile dimples in thicker metallic films,[15] and is inconsistent with void formation by grain pullout and similar mechanisms. With the exception of one sample, no evidence of Mg transfer to the glass substrate was found, which helps explain the relatively small amounts of metallic Mg exposed to the oxygen during peel (i.e., total cohesive failure should generate Mg site densities much greater than that of a flat, clean Mg surface).

Despite the relatively smooth appearance of the glass surfaces exposed during peel, these surfaces are still considerably rougher than the substrates employed in the deposition process. Figure 6 shows an AFM image of a glass substrate taken within hours of completing the cleaning process but prior to deposition. This increase in roughness suggests that crack growth is for the most part not confined to the interface adjacent to the glass.

AFM of the as-deposited Mg films gives some indication of the film microstructure, which may affect the deformation process. Typical AFM images of freshly deposited Mg are shown in Fig. 7. Note that in sample preparation, the imaged surfaces are coated with epoxy and thus do not correspond directly to the surfaces exposed during peel from the glass substrate. As-deposited, 1-μm films show a distinct plate-like structure, where the larger platelets are a few

hundred nm across and slightly inclined to the plane of the film. These films display diffuse reflectance, consistent with the lateral dimensions of the largest platelets. Where the edges of the platelets are exposed, a columnar structure is evident; growth columns in deposited material are generally a consequence of atomic shadowing during deposition on low temperature substrates.[16] Although one must be careful in deducing grain structure from AFM images, the plate-like microstructure observed is consistent with a polycrystalline HCP metal, where the plate surfaces are approximately aligned with the c-axis. A better indication of the film microstructure adjacent to the glass is perhaps achieved by examining much thinner films. Figure 7(b) shows an image of a very thin film in a region of the glass substrate shadowed from the evaporation source. The regions show very small (some tens of nm across) structures, consistent with their shiny appearance (specular reflection).

These AFM scans suggest that the grain structure of the film coarsens considerably with during deposition, starting with a fine grained structure near the glass interface and coarsening as deposition proceeds. In the initial stages of deposition, the microstructure of the surface appears to be similar to that of the peeled Mg films displaying low peel energies [comparing Figs. 4(b) and 7(b)] The Mg platelets on the 1-μm film are consistent with preferentially oriented grains. Platelet growth of this sort requires some sort of preferential growth mechanism, either due to mobility among the adsorbed Mg atoms or to preferential sticking of Mg on appropriately oriented surfaces. The as-deposited 1-μm film is much rougher than any of the peel surfaces, with a range in surface features of about 200 nm in this scan. This roughness would hinder deformation in the Mg near the epoxy and would thus reduce the thickness of the deformed portion of the Mg film.

DISCUSSION

Emission Process. Chemisorptive electron emission involves short-lived intermediate states formed as an electronegative atom or molecule (e.g., O, O_2, X, X_2—where X = halogen)

approaches the surface.[17-22] In the model developed by Nørskov, Newns, Lundqvist[23] and Kasemo et al.,[24] and elaborated by Prince and co-workers,[25-27] CSE is ascribed to an electron-tunneling-Auger emission sequence immediately prior to the collision of an approaching gas molecule with the surface. As the gas molecule approaches the surface, the energy of the lowest unfilled electron state (whose energy defines the electron affinity of the molecule, E_A) can drop significantly; if E_A falls below the Fermi level of the metal, E_F, an electron can tunnel from the metal to the molecule to produce a negative ion. If the tunneling probability is sufficiently low and the molecule approaches the surface with a sufficiently high velocity, there is a finite probability that E_A can fall well below E_F before tunneling occurs; i.e., the electronic states in the metal available for tunneling can lie a few eV below the Fermi energy. Electron tunneling from such a state produces a substantial excitation in the metal; if the energy of this excitation is greater than the metal work function, ϕ, its decay can yield electron emission. Thus the energetics of this electron emission mechanism requires that the work function be smaller than the difference between E_F and E_A, where E_A is measured very *near the metal surface*; i.e.,

$$\phi < E_F - E_A \qquad (1)$$

Although the probability of emission during the approach of a suitable molecule is quite low, CSE is readily observable for metals such as Mg, Ti, Zr, Al, and alkali metals exposed to gases such as oxygen and the halogens. CSE probabilities are typically ~ 10^{-6} or less per exposed metal atom. The integrated emission intensity is expected to be nearly proportional to the total area of freshly exposed metal.

Magnesium films were employed in this work due to the intense CSE signals resulting from exposure to oxygen. Instantaneous currents as high as 2×10^{-11} A/cm^2 (~1×10^8 e$^-$/cm^2/s) have been observed from Mg at somewhat lower oxygen pressures.[28] Although our sensitive detectors saturate at currents about a magnitude lower than this (for 1-2 cm^2 samples), we often detect significant emission thousands of seconds after the peel event.

The unusual intensity and duration of CSE from Mg is due to the extremely high affinity of Mg for oxygen, so that oxide islands are nucleated and grow upon the metallic surface.[29,30] This leaves small patches of low function material between the islands which persist after the absorption of oxyge equivalent to many monolayers. In the early stages of absorption, the work function of the surface actually decreases and reaches a minimum after exposures of several monolayers.[28,31] Since the CSE efficiency depends exponentially on the work function, the peak emission efficiency in Mg occurs after considerable exposure to O_2, consistent with observations in this work. Since we integrate over several hundred seconds of emission for both calibration and fracture experiments, none of these emission subtleties effect our conclusions.

Peel Mechanics. The ductility of thin metallic films sandwiched between brittle sheets is strongly constrained by the brittle sheets. Key parameters in the deformation process include the presence of microstructural defects which would nucleate ductile voids, the film thickness, and the presence of brittle phases along the interface (brittle interphases).[3] Evans and Dalgleish conclude that the density of nucleation sites is important whenever the average distance between nucleation sites, x, is less than about one tenth the film thickness, h ($x \leq h/10$). In the present work, the average distance between voids on typical high peel energy surfaces is generally greater than 1 μm ($x > h$). This is consistent with the very smooth glass surfaces used in sample preparation. Although grain boundaries in the metallic phase can serve as nucleation sites, this is apparently not the case in this material system. In the absence of effective nucleation sites, voids can be still nucleated by plastic instabilities ahead of the crack tip; this typically requires local stresses on the order of five times the yield stress.[3] The high stress required for void nucleation under these conditions would favor brittle failure along any weak interface or interphase, should they be present.

The film thickness can also affect deformation by virtue of its affect on the yield strength of the metallic phase. Embury and Hirth conclude that yield in sub-μm films is controlled by the motion of screw dislocations, where the yield stress, σ_y, scales as the reciprocal of the film thickness, h ($\sigma_y \sim h^{-1}$).[32] Thus, yield becomes more difficult as the film thickness decreases,

and a transition to brittle failure, either along an interface or an interphase, becomes more likely. With few exceptions, the 0.5-μm films tested in this work failed in a brittle fashion with very little CSE, consistent with a high yield stress which favors other fracture modes (here, brittle failure through an interphase). Presumably thinner films would display even more consistent brittle failure. The 1-μm films employed in this work appear to be marginally ductile, in the sense that the film thickness is barely sufficient for substantial ductility. The marginal ductility of these films may help account for the variability observed in the peel energies, where small differences in the material parameters and loading conditions would significantly modify the peel mechanics.

Even in the 1-μm films, failure appears to be largely brittle when reckoned as a fraction of the nominal surface area. The lowest peel energies observed in this work are about 3 J/m^2. This is similar to the fracture energy of single crystal MgO [along (100) cleavage planes][33] and is thus consistent with the presence of a brittle oxide interphase. By way of contrast, the fracture energy of soda lime glass is significantly higher, about 9 J/m^2, inhibiting crack growth through the glass phase (parallel to the interface). Crack growth through the glass phase (or through the Mg phase) parallel to the Mg-glass interface would require pure Mode I conditions at the crack tip, i.e., $K_{II} = 0$. ($K_{II} \neq 0$ would produce curvature.) Although the $K_{II} = 0$ condition can be met by some material combinations, the analysis of Hutchinson, Mear, and Rice indicates that the elastic constants of Mg and glass are incompatible with the $K_{II} = 0$ condition, at least for the case of symmetric wedge loading.[34] Since a relatively small amount of fresh surface Mg is actually exposed even in the high peel energy samples, we conclude that crack growth proceeds largely through a brittle interphase, and that ductile voiding disrupts this layer in the high peel energy samples.

AFM images of metallic films displaying significant CSE signals and high peel energies characteristically displayed large numbers of angular voids. These features are distinctly unlike the ellipsoidal voids characteristic of ductile failure of bulk metals and thicker metal films. These voids are probably embryonic forms of the ellipsoidal voids which have not developed

completely due to the thinness of the film. The formation of smooth ellipsoidal features in Mg (HCP structure) is further hindered (relative to the FCC metals) by the lack of the five equivalent slip planes required for arbitrary deformations.[15]

Roughness vs Peel Energy. AFM observations of fracture surfaces have found increasing application in providing quantitative information on fracture mechanisms and fracture toughness. In materials systems with a single toughening mechanism, quantitative measures of the surface topology can often be related to the fracture energy, for example in steels[35] and some ceramics.[36] In principle, AFM images can be processed to yield the total surface area—which would provide an alternative measure of deformation in thin films. However, area measurements (and other quantitative measures derived from fracture surface images) often suffer from a "magnification effect,"[37] where the parameter of interest (e.g., area or roughness) is a strong function of the magnification employed, even in the limit of high resolution. Nevertheless, such measurements are often useful when the parameter is independent of magnification over some range of magnifications, or when some physical scaling relation can be found.[37,38]

Using AFM data, we examined the roughness of the metal fracture surface as a possible parameter to compare with peel energy, employing the mean surface roughness defined in Eq. 1 as the roughness measure. Figure 8 shows the mean surface roughness of several peeled Mg surfaces as a function of scan size on a log-log scale. Each point represents an average of the roughness of 3-4 scans at different positions on the indicated sample at the indicated scan size. In each of the samples studied, the roughness increases with scan size and plateaus in the limit of large scan sizes. Very similar results were obtained using the root-mean-square roughness.[39] The increase in roughness with scan size reflects the presence of large features (features which cover larger areas) which display large deviations from the mean surface position; consequently they dominate the surface roughness. However, large scans often do not sample the small scale roughness adequately, and thus at sufficiently large scan sizes, the roughness can actually decrease. This is especially the case in most commercial AFM instruments, including the one

employed here, which utilize a fixed number of scans and a fixed number of points per scan (here 256×256).

If the samples in Fig. 8 are ranked by roughness (at the maximum value of roughness) a moderate correlation with peel energy is observed, reflecting an expected correlation between the size and number of ductile voids (the largest features observed on the surface) with the peel energy. However, the roughness of the 10 J/m^2 sample is anomalously high, suggesting that the correlation also depends on other factors, e.g., the distribution of void sizes. Nevertheless, alternative approaches for acquiring and analyzing AFM data from these metal surfaces may yet prove useful.

One difficulty presented by these particular surfaces is the tremendous range of relevant scale lengths, from atomic steps (associated with the Burgers vectors of individual dislocations) to the dimensions of the ductile voids (some hundreds of nm in diameter). To properly sample the ductile voids while maintaining adequate resolution for atomic steps requires far more height measurements per scan than provided by most AFM instruments. Proper characterization may be impossible if true atomic resolution is required, due to the finite tip radius. Atomic or near-atomic resolution, when it has been achieved, has been achieved on much smoother surfaces than the Mg surfaces in this study. In particular, we expect that the highest step densities along the sidewalls of the ductile voids. Imaging these steep walls with the required resolution may prove a formidable challenge.

The non-ferrous metals display a wide range of deformation behaviors which may allow a variety of experimental approaches. FCC metals, such as Al, tend to deform more homogeneously (due to local strain hardening) and yield smoother (although often larger) surface surfaces. In contrast, the HCP metals, such as Mg, Ti, and Zr, tend to deform more inhomogeneously (due to local strain softening) and produce rougher surfaces. CSE measurements on these materials would yield reproducible surface area values despite the contrasting morphologies.

Chemisorptive emission as a probe of deformation. For the system presented here, the CSE intensities appear to be more directly related to Mg deformation processes than the large scale surface roughness. Since CSE is an atomic scale process, CSE intensities should clearly reflect the amount of metallic surface exposed during the peel event. This proportionality may be exploited to provide a measure of deformation energy in thin films of reactive metals. The close relation been measured peel energy in the failure of Mg/glass interfaces certainly bears this out, since the principal mechanism for the enhancement of peel energy is deformation in the metal phase. This close relation can be attributed to the general correlation between steps created on the fracture surface and the deformation process.

The relation between the creation of surface area and the work of deformation can be illustrated in a very simple geometry shown in Fig. 9. Consider an edge dislocation of length l oriented parallel to the surface and moving into the material along a direction perpendicular to the surface. For simplicity, we assume that the Burgers vector is oriented normal to the surface, so as to produce a vertical step. The material on either side of the plane of the dislocation is displaced a distance b, the magnitude of the Burgers vector, and the force producing this displacement is on the order of the yield stress σ_y, times the area swept out by the dislocation, $l \cdot d$, where d is the distance the dislocation has traveled into the material. Thus the total work of deformation is on the order of $\sigma_y \cdot b \cdot d \cdot l$.. Such a dislocation will create a step with area $\Delta A \approx b \cdot l$ on the surface. Then the ratio between the plastic work of deformation and total surface area (ΔA) produced by deformation will be on the order of $\sigma_y \cdot d$. Expressing this relation in terms of work per unit surface area, we find

$$\frac{W_{plastic}}{A} \approx \sigma_y \cdot d \frac{\Delta A}{A} , \qquad (2)$$

where $W_{plastic}/A$ is the work of plastic deformation per unit area, and $\Delta A/A$ is the ratio between the surface area produced by deformation and the nominal area of the peeled surface. This line of reasoning essentially equates $\Delta A/A$ with the effective strain at failure, ε_0, where one expects

$W_{plastic}/A \sim \sigma_y \cdot d \cdot \varepsilon_0$ and d is the depth of the deformed material. In thin film systems where the distance between void nucleation sites is not much less than the film thickness, it generally adequate to assume that the film is uniformly deformed throughout its thickness ($d = h$).[3]

In this work, the maximum observed peel energy was about 16 J/m^2; assuming that the work of plastic deformation equals the difference between the observed peel energy and the lowest observed peel energy (the zero deformation limit), $W_{plastic}/A \approx 13$ J/m^2 for this sample . From the CSE measurements, we estimate that the corresponding $\Delta A/A$ was 0.16. Yield measurements on bulk Mg indicate that $\sigma_y \approx 100$ MPa. Assuming that d equals the full thickness of the film (1 μm), we find that $\sigma_y \cdot d \cdot \Delta A/A \approx 16$ J/m^2. In view of the assumptions involved, this agrees well with $W_{plastic}/A$. We therefore conclude that the CSE measurements are indeed probing surface area changes which closely reflect the total amount of plastic deformation in the film.

Although this analysis was applied to very thin films, we expect that the same considerations will apply to thicker metallic structures as long as the thickness is smaller than the expected depth of plastic deformation in the metallic phase. For most ductile metals, this is in excess of 10 μm, and for very ductile metals (e.g., Al) may be as large as 100 μm. Thus the technique may prove quantitatively useful in the study of practical ceramic-reinforced, metal matrix composites, e.g., Al_2O_3-reinforced Al, as long as the thickness of the metallic phase is not to great. [Several commerical Al_2O_3-Al composites have inter-particle distances in the 5-50 μm range.] In cases where the thickness of the metal phase is significantly greater than the extent of the deformed region, allowance must be made for possible variations in the thickness of the deformation (corresponding to d in Eq. 1). If TEM measurements show that this variation is not great, i.e., a d_{avg} is meaningful, then quantitative determinations of the work of plastic deformation based on CSE measurements would be valid in these materials as well.

CONCLUSIONS

The energy expended during the peel of thin Mg films from glass substrates can be strongly enhanced by deformation in the metallic phase. Samples displaying the lowest peel energies yielded very low CSE emission intensities, implying that the fracture energy of these samples was dominated by failure through a brittle interphase. Samples displaying higher peel energies yielded higher CSE intensities and nm-scale voids, detected by AFM of the fracture surface, consistent with the nucleation and growth of ductile voids ahead of the crack tip. It is likely that these small voids are the precursors of the elliptical dimples produced during ductile failure of less constrained metallic materials. As a quantitative probe of plasticity, AFM roughness measurements are problematic due to the wide range of scales required for proper characterization. Novel acquisition methods, such as wide scan, extremely high digitization densities, may solve these problems. STM (due to its very high lateral resolution) of these very rough surfaces, although difficult, may also be an important tool. [Warner and Bonnell[40] have reported the use of STM to examine the metal side of a bimaterial interface fracture and saw correlations between the observed topography and fracture energy.]

Chemisorptive electron emission intensities following the failure of Mg/glass samples during slow peeling are strongly correlated with the peel energies determined from load curves. Simple peel energy estimates based on the CSE intensities, assuming that the measured increase in surface area is entirely due to deformation, are in substantial agreement with the measured peel energies. Thus CSE measurements have considerable potential as a probe of deformation in material and process evaluation, due to their ability to sense the contribution of the most important toughening mechanism in metal-ceramic components. This is particularly valuable in systems where the relative contribution of other competing fracture processes (e.g., fracture through a brittle interphase, fracture of brittle reinforcements) is variable or not known. We expect that this technique can be readily extended to thicker metallic phases and to other reactive metals, including Ti, Zr, and Al, and commercially important metal-ceramic composites. Over a rather broad range of sample parameters, CSE intensities provide a quantitative measure of the integrated work of deformation over the entire fracture surface.

ACKNOWLEDGMENTS

We thank John Hirth for helpful discussions and Wenbiao Jiang for performing x-ray measurements on the deposited films. This work was supported by the Air Force Office of Scientific Research Contract No. AFOSR-F49620-91-C-0093, National Science Foundation Instrumentation Grant DMR-9201767, the Murdock Charitable Trust, and the Japan Private School Promotion Foundation.

REFERENCES

1. A. G. Evans and J. W. Hutchinson, Acta Metall. 37, 909 (1989).
2. Z. Chen and J. J. Mecholsky, Jr., J. Mater. Res. 8, 2362 (1993).
3. A. G. Evans and B. J. Dalgleish, Mater. Sci. Engin. A162, 1 (1993).
4. J. Kim, K. S. Kim, and Y. H. Kim, J. Adhesion Sci. Technol. 3, 174 (1989).
5. A. G. Evans, B. J. Dalgleish, M. He, and J. W. Hutchinson, Acta Metall. 37, 3249 (1989).
6. I. E. Reimanis, B. J. Dalgleigsh, and A. G. Evans, Acta Metall. Mater. 39, 3133 (1991).
7. J. T. Dickinson, L. C. Jensen, S. C. Langford, and R. G. Hoagland, J. Mater. Res. 9, 1156 (1994).
8. B. Sujak and A. Gieroszyński, Acta Phys. Polon. 28, 249 (1968).
9. W. J. Baxter, Fatigue Engin. Mater. Struc. 1, 343 (1979).
10. O. F. Hagena, G. Knop, R. Fromknecht, and G. Linker, J. Vac. Sci. Technol. A 12, 282 (1994).
11. Yoshihisa Watanabe, Yoshikazu Nakamura, J. T. Dickinson and S. C. Langford, "Changes in air-exposed fracture surfaces of silicate glasses observed by atomic force microscopy," to appear in J. Non-Cryst. Solids.
12. L. A. K'Singam, J. T. Dickinson, and L. C. Jensen, J. Am. Ceramics Soc. 68, 510 (1985).

13. D. L. Doering, S. C. Langford, J. T. Dickinson, and P. Xiong-Skiba, J. Vac. Sci. Technol. A. 8, 2401 (1990).

14. Richard W. Hertzberg, *Deformation and Fracture Mechanics of Engineering Materials*, 3rd Ed. (John Wiley, New York, 1989), pp. 81-83.

15. A. G. Evans and B. J. Dalgleish, Acta Metall. Mater. 40, S295 (1992).

16. J. A. Thorton, J. Vac. Sci. Technol. A 4, 3059 (1986).

17. B. M. McCarroll, J. Chem. Phys. 50, 4758 (1969).

18. B. Kasemo, E. Törnqvist, and L. Walldén, Mater. Sci. Engin. 42, 23 (1980).

19. R. H. Prince and R. Persaud, Surf. Sci. 207, 207 (1988).

20. R. H. Prince, R. M. Lambert, and J. S. Foord, Surf. Sci. 107, 605 (1981).

21. M. A. Loudiana, J. Bye, J. T. Dickinson, and D. A. Dickinson, Surf. Sci. 157, 459 (1985).

22. I. V. Krylova, Poverkhnost Fiz. Khim. Mekhan. 1, 5 (1988).

23. J. K. Nørskov, D. M. Newns, and B. I. Lundqvist, Surf. Sci. 80, 179 (1979).

24. B. Kasemo, E. Törnqvist, J. K. Nørskov, and B. I. Lundqvist, Surf. Sci. 89, 554 (1979).

25. R. H. Prince, R. M. Lambert, and J. S. Foord, Surf. Sci. 107, 605 (1981).

26. M. P. Cox, J. S. Foord, R. M. Lambert, and R. H. Prince, Surf. Sci. 129, 399 (1983).

27. E. B. Deblasi Bourdon and R. H. Prince, Surf. Sci. 144, 591 (1984).

28. T. F. Gessell, E. T. Arakawa, and T. A. Callcott, Surf. Sci. 20, 174 (1970).

29. H. Namba, J. Darville, and J. M. Gilles, Surf. Sci. 108, 446 (1981).

30. G. C. Allen, P. M. Tucker, B. E. Hayden, and D. F. Klemperer, Surf. Sci. 102, 207 (1981).

31. T. F. Gessell and E. T. Arakawa, Surf. Sci. 33, 419 (1972).

32. J. D. Embury and J. P. Hirth, "On dislocation storage and the mechanical response of fine scale microstructures," pre-publication.

33. J. J. Mecholsky, Jr., S. W. Freimam, and R. W. Rice, J. Mater. Sci. 11, 1310 (1976).

34. J. W. Hutchinson, M. E .Mear, and J. R. Rice, J. Appl. Mech. 54, 828 (1987).

35. B. B. Mandelbrot, D. E. Passoja, and A. J. Paullay, Nature 308, 721 (1984).

36. J. J. Mecholsky, D. E. Passoja, and K. S. Feinberg-Ringel, J. Am. Ceramic Soc. 72, 60 (1989).

37. E. E. Underwood and K. Banerji, Mater. Sci. Engin. 80, 1 (1986).

38. J. L. Chermant and M. Coster, J. Mater. Sci. 14, 509 (1979).

39. R. S. Sayles, in *Rough Surfaces*, T. R. Thomas, ed. (Longman, London, 1982), p. 92.

40. C. P. Warner and D. A. Bonnell, Materials Research Society Symposia Proceedings 237, 393(1992).

FIGURE CAPTIONS

FIG. 1. Diagram of the (a) apparatus employed in the CSE measurements and (b) geometry of the peel sample.

FIG. 2. Typical CSE signals following peel of Mg films from soda-lime glass: (a) a 1-μm film deposited on a room temperature substrate, (b) a 0.5-μm film deposited on a room temperature substrate. The partial pressure of O_2 was lowered from 4×10^{-4} Pa to about 7×10^{-6} Pa twice in (a) and once in (b).

FIG. 3. A plot of CSE intensities vs peel energy, where the CSE intensities are given by the total number of electrons detected beginning 50 s after the peel event and ending 1200 s later. The line represents the least squares fit to the data from the 1-μm films only.

FIG. 4. AFM images of peeled Mg surfaces: (a) the 1-μm film yielding the intense CSE shown in Fig. 2(a), and (b) the 0.5-μm film yielding the very weak CSE shown in Fig. 2(b).

FIG. 5. AFM images of the glass surfaces exposed during the peel of (a) the 1-μm film yielding the intense CSE shown in Fig. 2(a), and (b) the 0.5-μm film yielding the very weak CSE shown in Fig. 2(b).

FIG. 6. AFM image of a glass slide made after the cleaning treatment but before deposition of a metallic film.

FIG. 7. AFM images of the surface of an evaporated Mg film deposited at room temperature, (a) taken in the central portion of the film, where the film thickness is about 1 μm, and (b) taken in a region of the substrate shadowed from the deposition source, where the film is much thinner. Region (b) has a visibly mirror-like finish, while Region (a) displays diffuse reflectance.

FIG. 8. A plot of the measured mean surface roughness as a function of scan size for five samples with the indicated peel energies. All scans employed in the roughness measurements were made within 6 hours after removing the samples from the vacuum system.

FIG. 9. Diagram of idealized dislocation geometry demonstrating the relation between the change in thin film surface area accompanying deformation and the work of deformation. An edge dislocation of length l is associated with a vertical step of height b on the surface, and has moved a distance d downward into the metallic film.

(a) Apparatus for CSEE Measurements

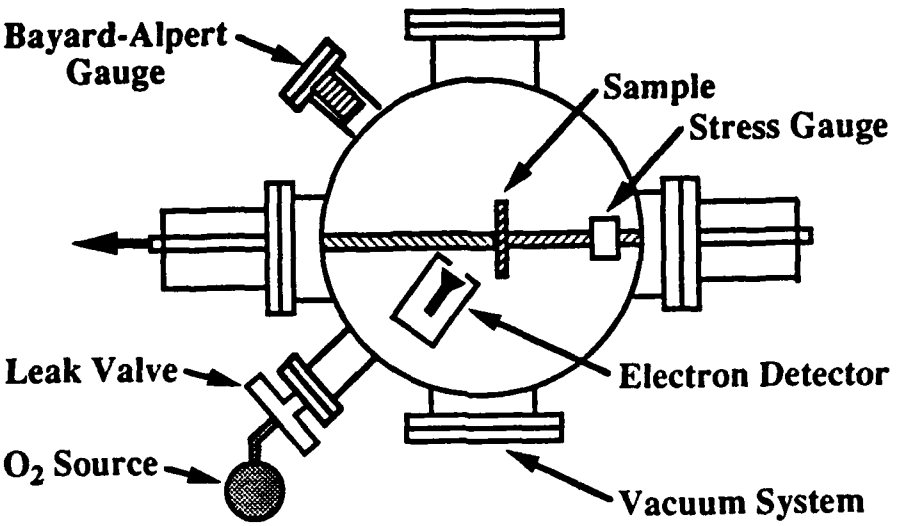

(b) Sample Geometry

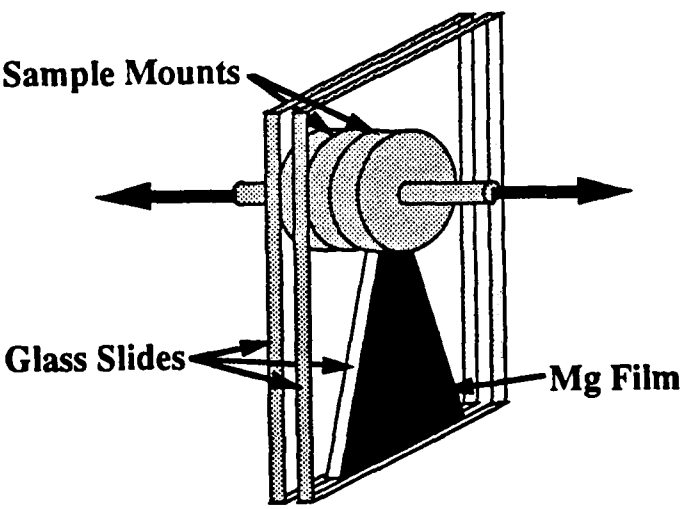

FIG. 1

Chemi-emission Intensities accompanying Peel of Mg from Glass

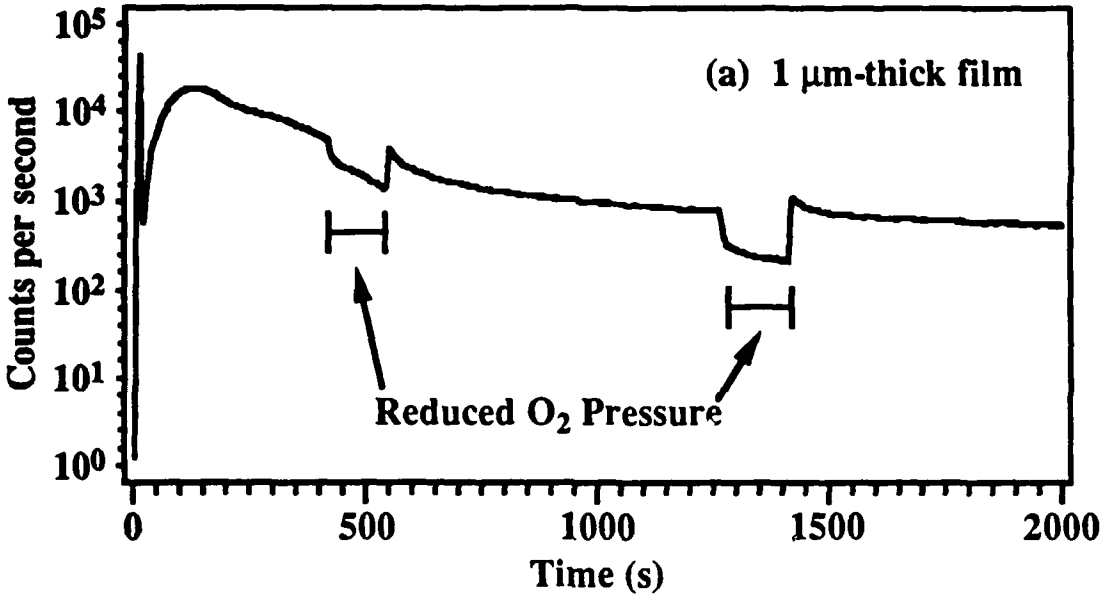

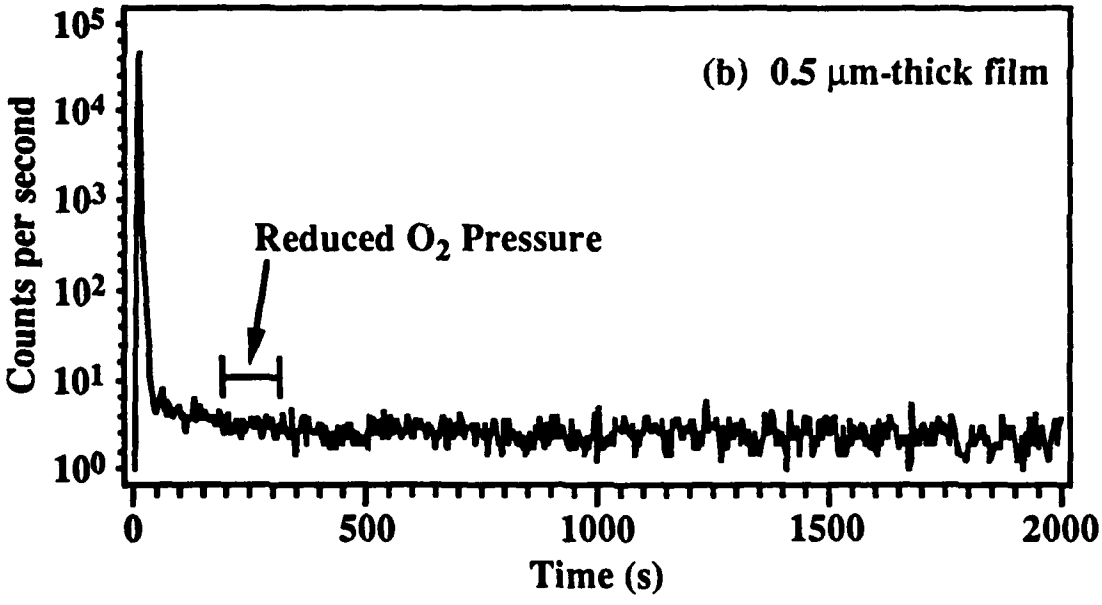

FIG. 2

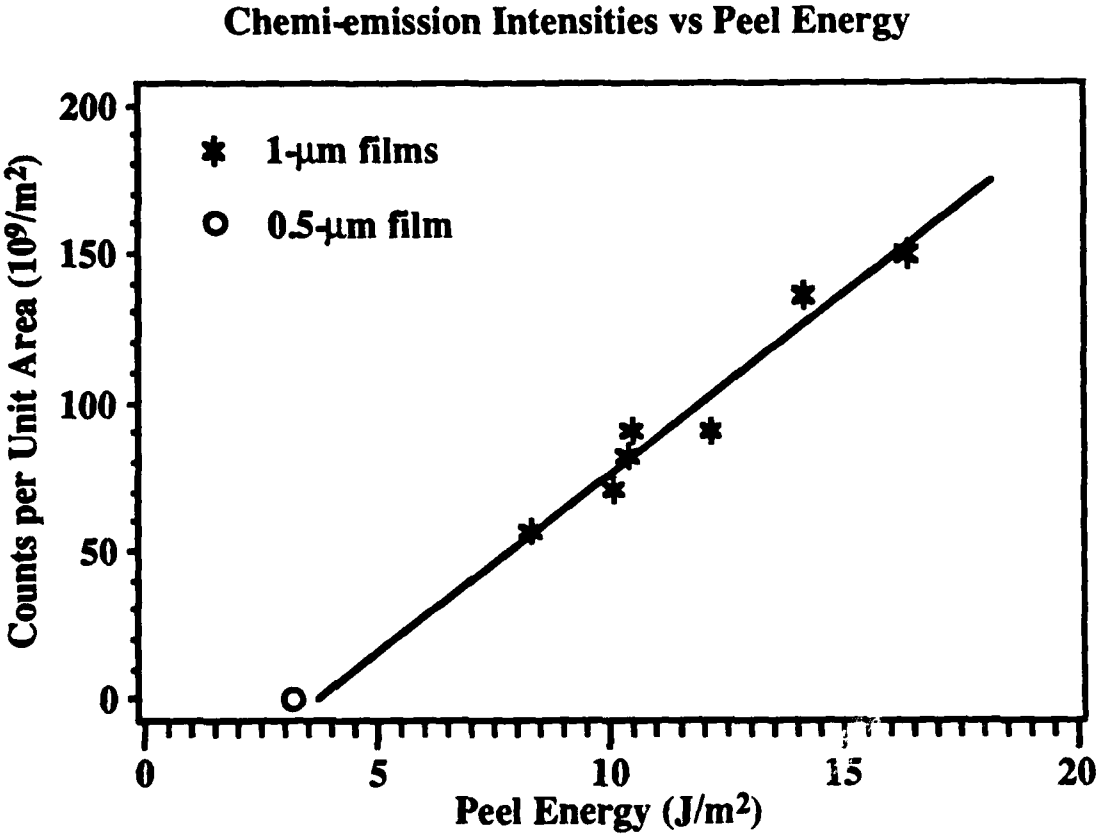
Chemi-emission Intensities vs Peel Energy
Counts per Unit Area ($10^9/m^2$)
200
150
100
50
0
1-μm films
0.5-μm film
0
5
10
15
20
Peel Energy (J/m^2)

FIG. 3

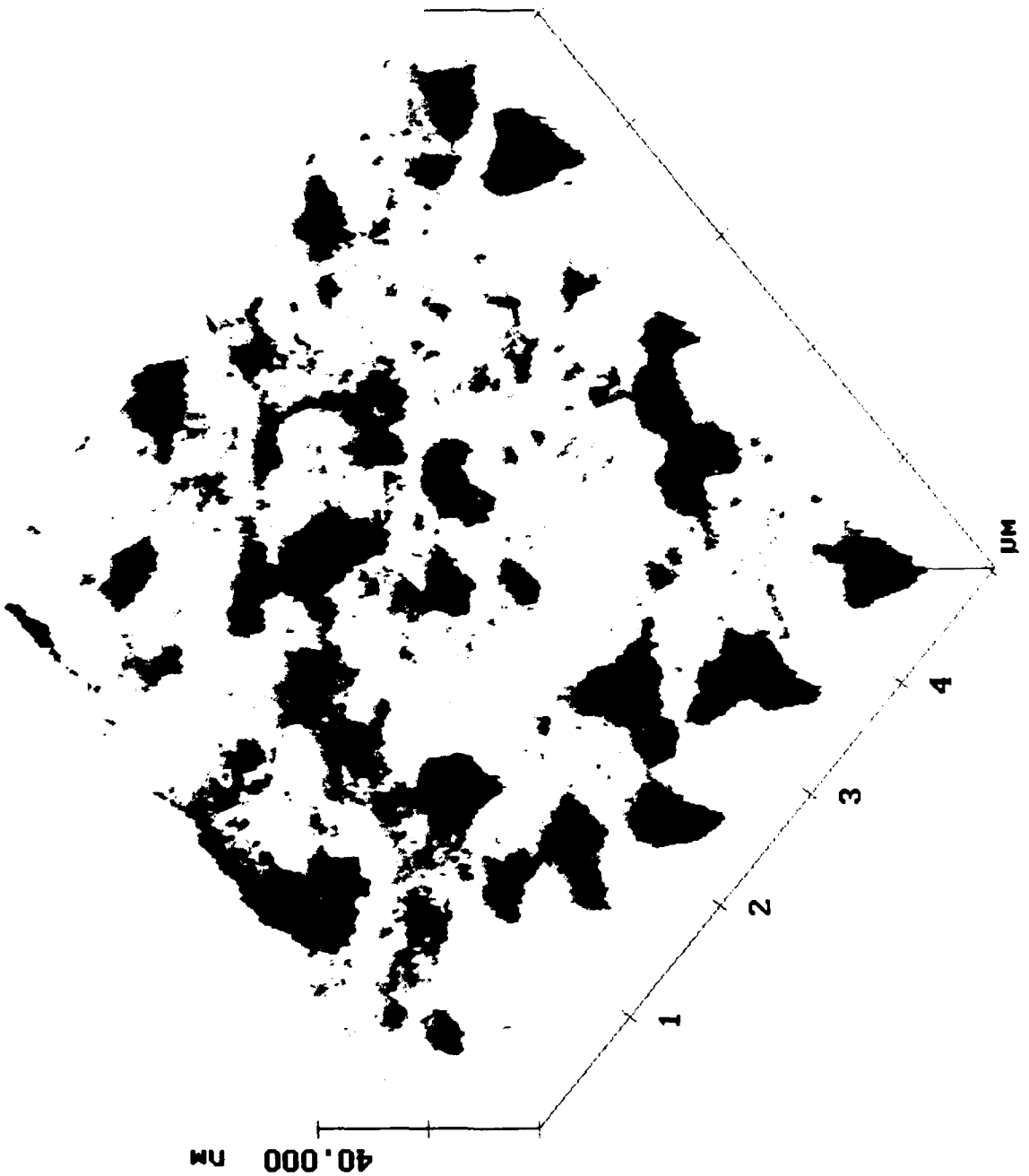

FIG. 4(a)

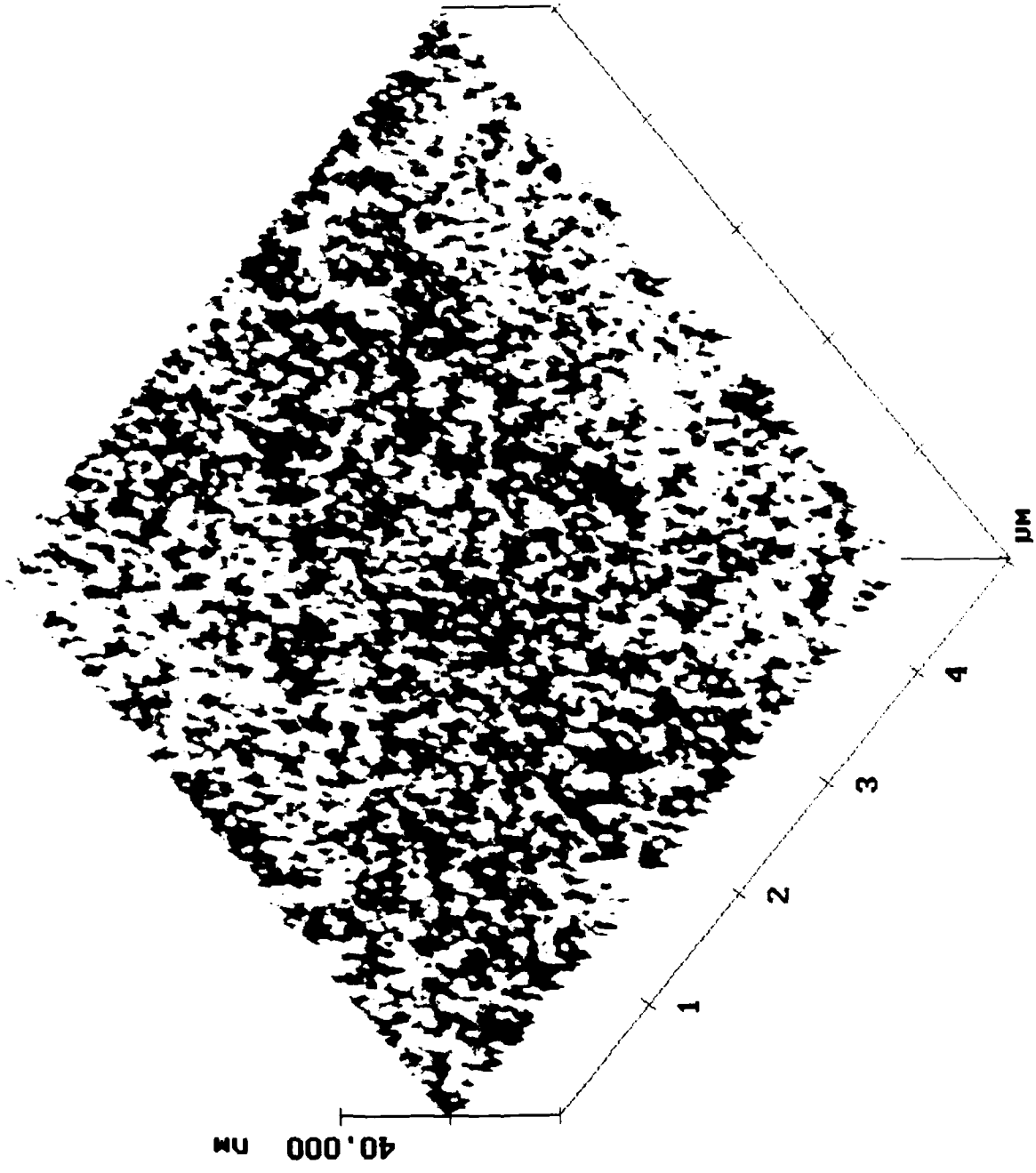

FIG. 4(b)

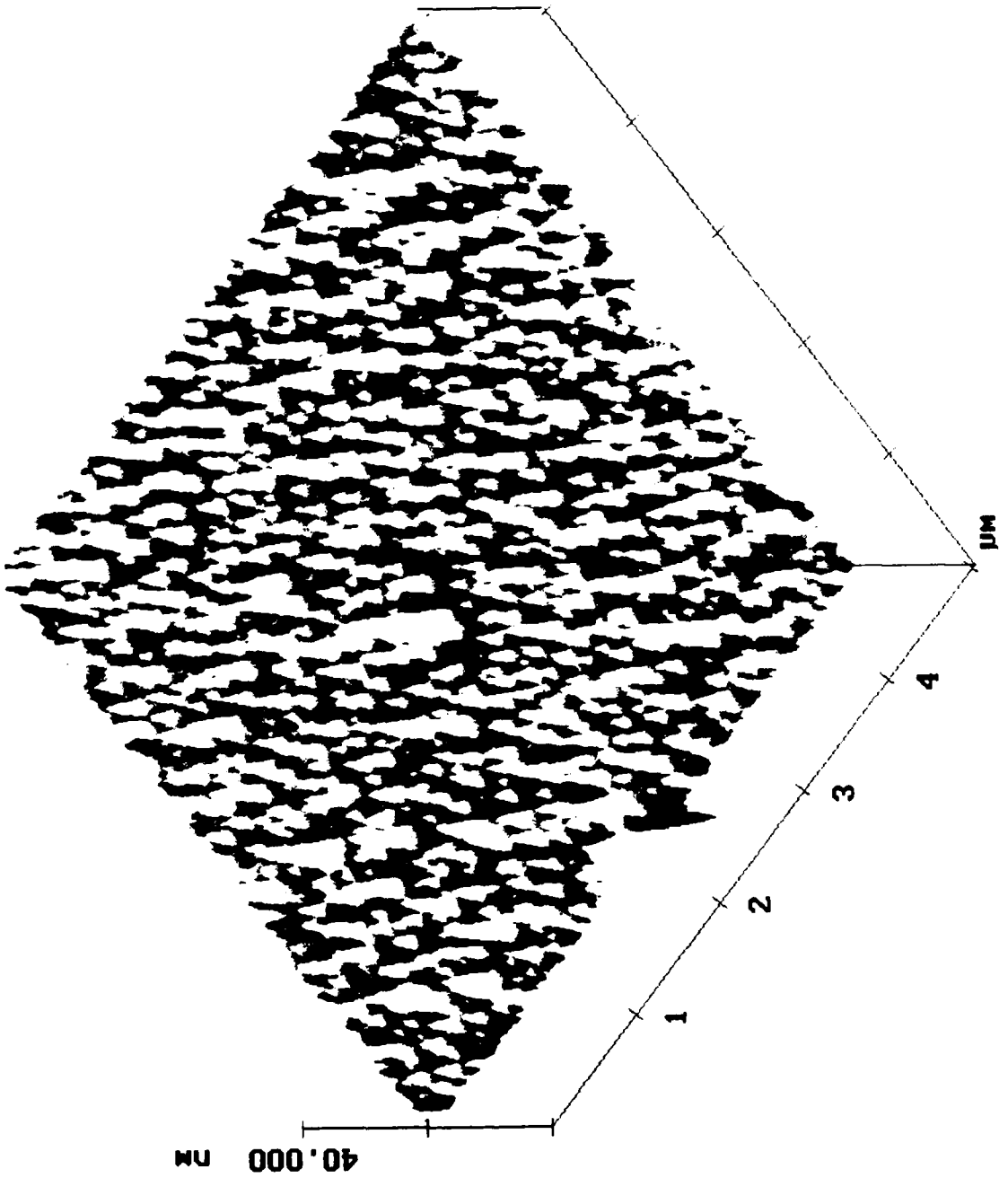

FIG. 5(a)

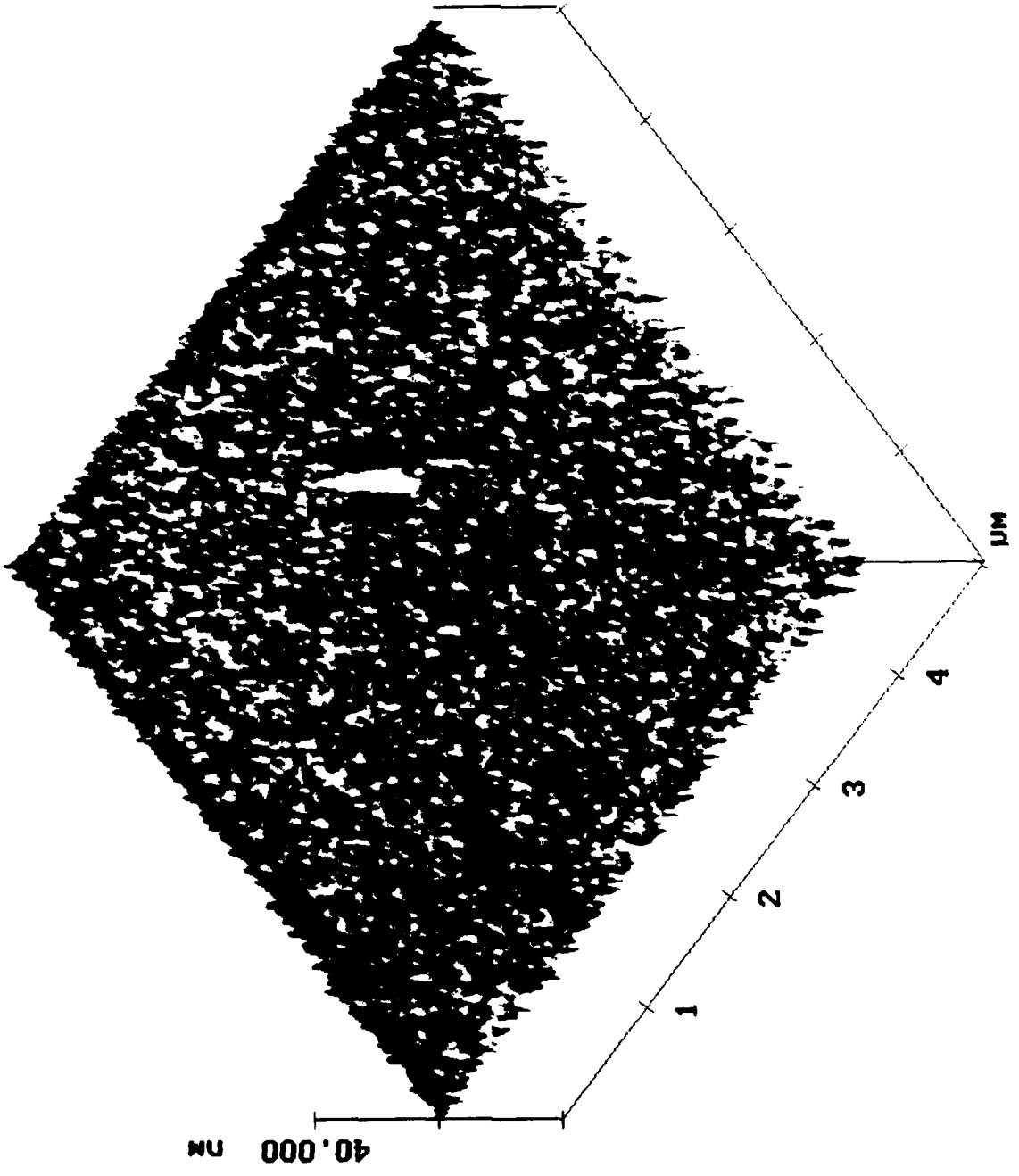

FIG. 5(b)

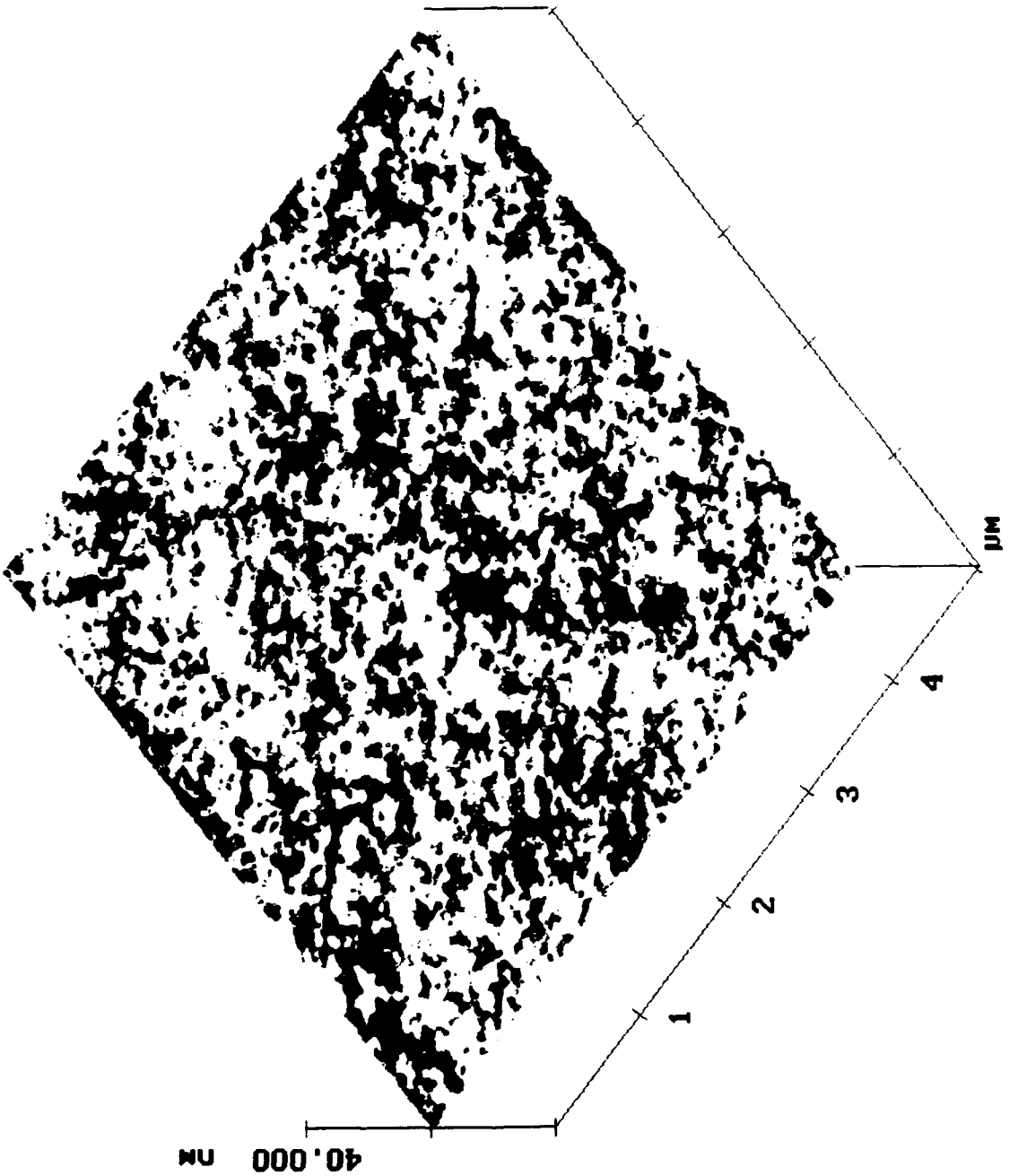

FIG. 6

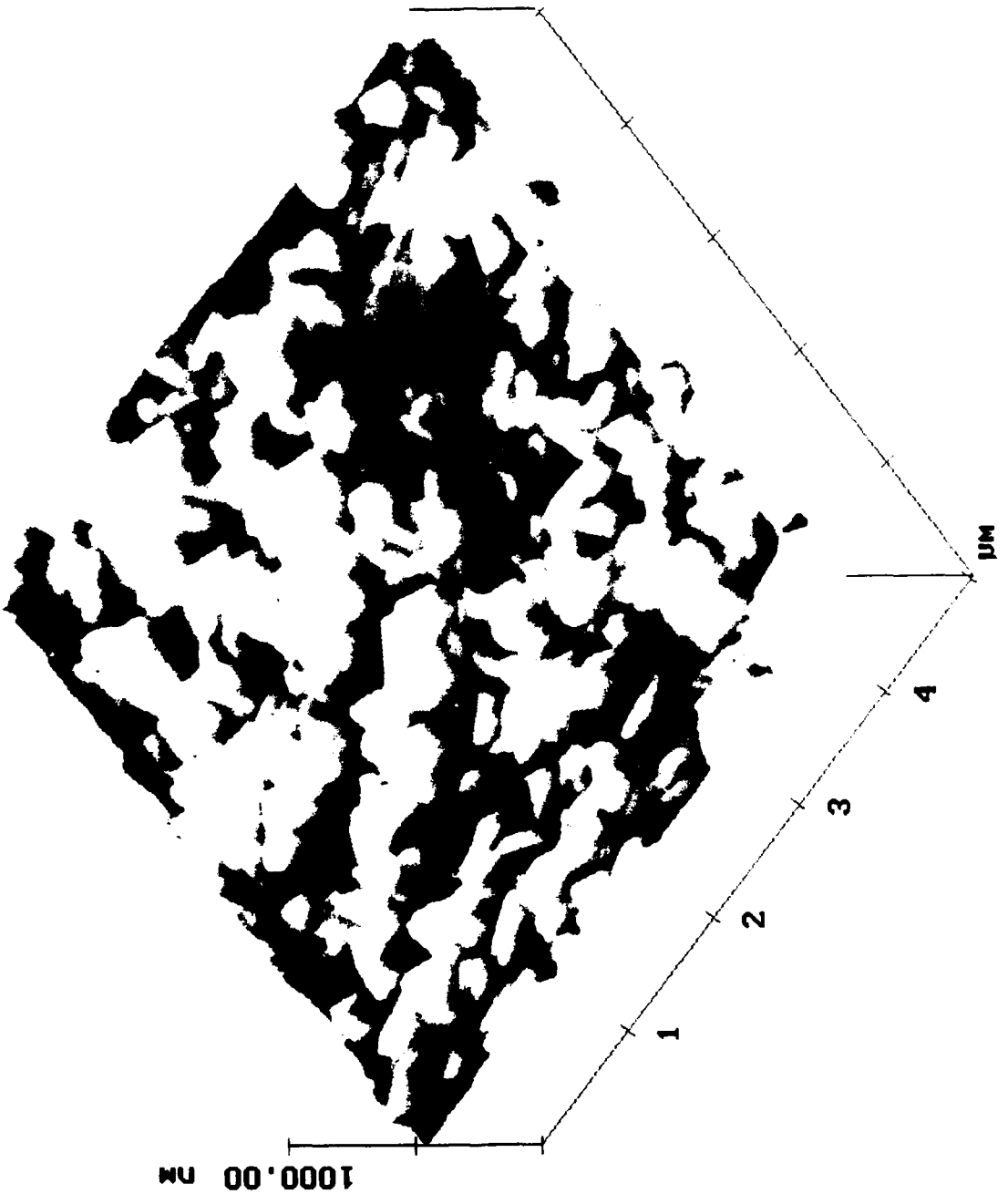

FIG. 7(a)

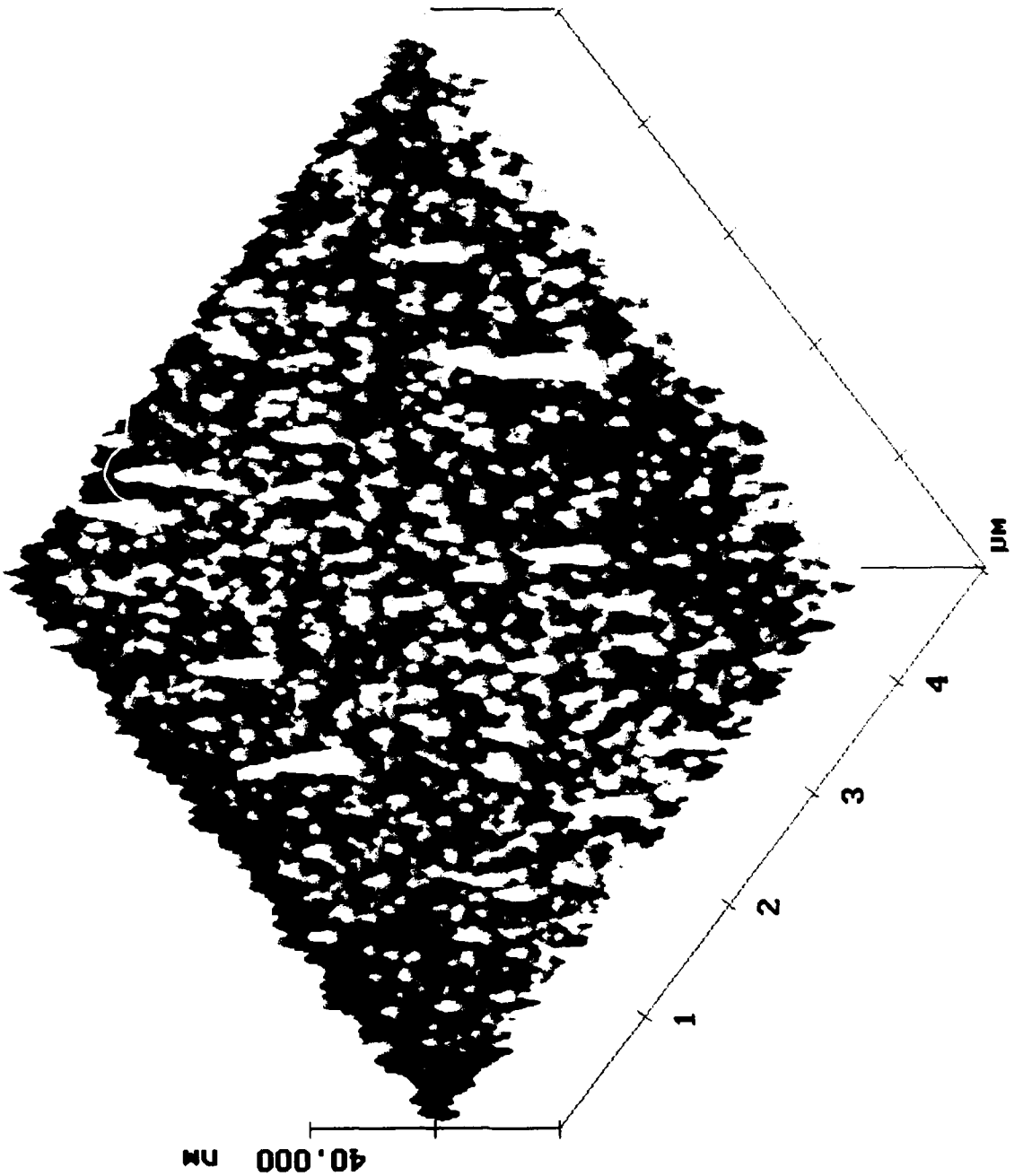

FIG. 7(b)

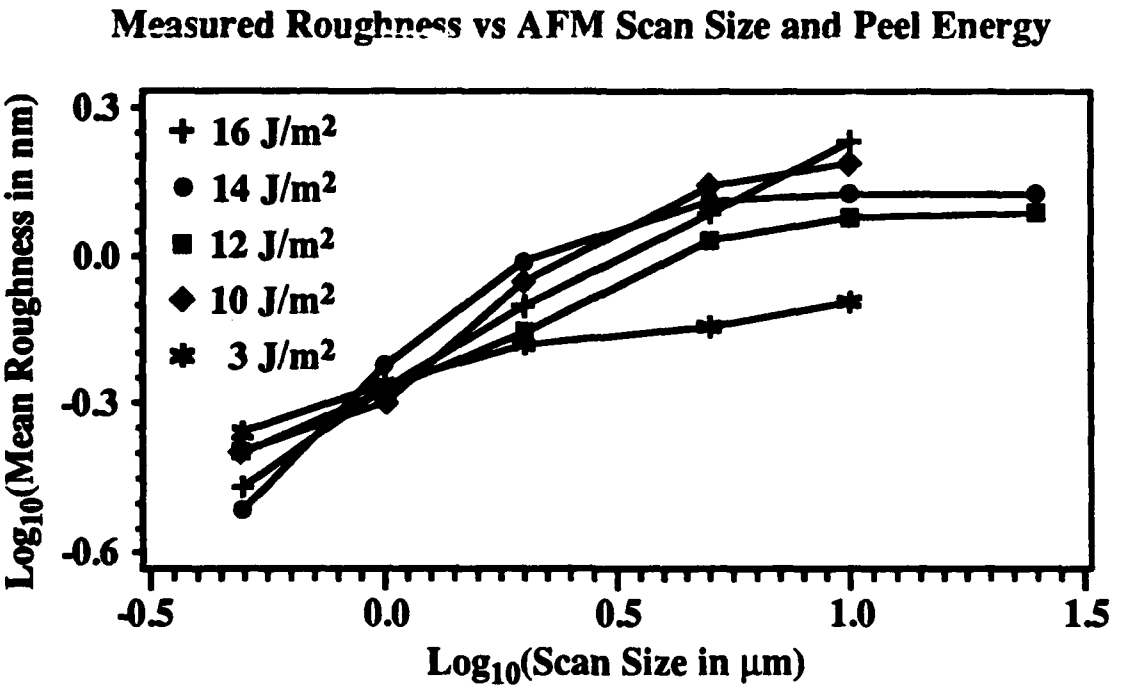
Measured Roughness vs AFM Scan Size and Peel Energy
+ 16 J/m2
● 14 J/m2
■ 12 J/m2
◆ 10 J/m2
✱ 3 J/m2
0.3
0.0
-0.3
-0.6
-0.5
0.0
0.5
1.0
1.5
Log10(Mean Roughness in nm)
Log10(Scan Size in μm)

FIG. 8

Dislocation Geometry for Simple Deformation Model

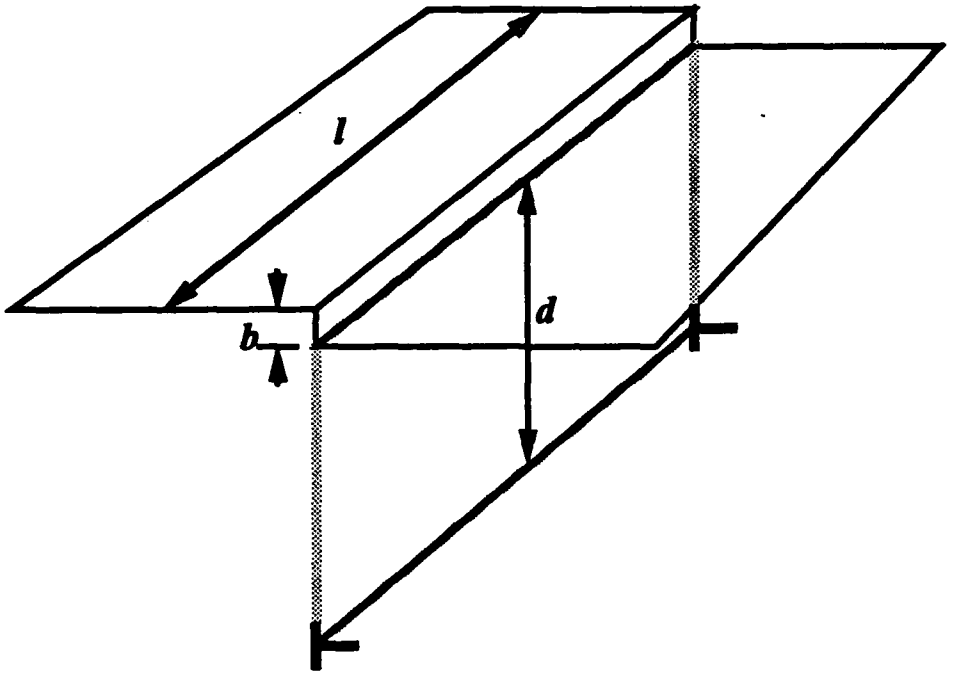

FIG. 9